January 2019

Distributed Optimal Power And Voltage Management In Dc Microgrids

Eyad A. Sindi
Wayne State University, sindi.eyyad@gmail.com

Recommended Citation

DISTRIBUTED OPTIMAL POWER AND VOLTAGE

MANAGEMENT IN DC MICROGRIDS

by

EYAD A SINDI

DISSERTATION

Submitted to the Graduate School,

of Wayne State University,

Detroit, Michigan

in partial fulfillment of the requirements

for the degree of

DOCTOR OF PHILOSOPHY

2019

MAJOR: ELECTRICAL ENGINEERING

Approved by:

_____

Adviser   Date

_____

Date

_____

Date

_____

Date

ACKNOWLEDGEMENT

I would like to express my sincere appreciation to Professor Le Yi Wang, who contributed tremendous time to my research. I would also like to express my deepest gratitude for his exceptional guidance and consistent support during my graduate study. His support and guidance were crucial for the completion of this work.

Appreciation is also due to Professor George Yin, Professor Feng Lin, and Professor Caisheng Wang for their constructive comments and valuable suggestions.

Special thanks to my parents, my brothers and my sister for their love and continuous support.

Most of all, I would like to express my appreciation to my wife LUTFIA for her love and encouragement. Thanks for her understanding, staying by my side and taking care of our baby boy.

TABLE OF CONTENTS

v

LIST OF TABLES

LIST OF FIGURES

vii

1 INTRODUCTION

Power systems are inherently networked systems. Increased penetration of renewable and distributed generators (DGs), controllable loads, energy storage systems, and advanced power electronics systems have ushered in a new paradigm of microgrids (MGs) on distribution networks [1, 2].

Centralized, decentralized, and distributed control methodologies have been developed to regulate frequency, control voltage profiles, reduce production costs, minimize power losses, and enhance reliability. Centralized control schemes employ a central processing unit to communicate with all generators and loads [3, 4]. To support plug-and-play of generators and loads without increasing overwhelmingly system complexity [5], decentralized or distributed control methods become desirable [6, 7, 8].

1 Problems Statement

For DC MGs, load allocation to distributed generators, line losses, and voltage profiles are intimately coupled. Achieving a suitable balance among these objectives is essential for reliable and efficient MG operations and imposes a significant challenge for control strategy development.

The problem in this work is to develop a distributed optimization strategy that would address these challenges while achieving the global optimal solution. Continuing on the work on distributed optimization algorithms, the second part of the problem will consider subsystem dynamics in DC microgrids.

1 Objective And Motivation

The motivation behind the work is to develop a new distributed control strategies for integrated management of load power sharing, line loss reduction, and voltage quality improvement in DC microgrids.

The first objective is to achieve a multi-objective optimization strategy that addresses the challenge of achieving a suitable balance among the competing objectives of bus current balance, power loss reduction, and voltage deviation attenuation. These objectives are expressed in a global optimization performance index. The corresponding global optimal solutions are derived. To reduce operational costs, improve robustness and reliability, and provide scalability, distributed optimal solutions are sought for this combined power management problem.

The second objective is to consider DC microgrids with subsystem dynamics. Inclusion of subsystem dynamics accommodates many real systems. impacts performance significantly, and complicates system analysis. Expanded dynamics systems are derived, and stability and convergence analysis are carried out, and the main properties are established.

This work shows that by designing suitable local optimization criteria and recursive algorithms, our distributed recursive algorithms are convergent to the global optima.

The control methodology of this work offers some distinct advantages: (1) It requires only neighborhood information exchange among nodes in the network. (2) The

local optimization can achieve global optimization. This is especially important for a large network with physically distributed subsystems. (3) It has provable properties of convergence to the global minima under noisy observations. (4) It is robust against load perturbations and allows reconfiguration with subsystem addition and deletion. (5) It is scalable in the sense that system expansion will not significantly increase control system complexity.

1 Literature Review

In comparison to the existing literature, it is first noted that this work integrates three performance objectives. Due to technical difficulties, traditional power systems decompose control tasks into decoupled problems, although the underlined physical systems are still highly coupled. For example, economic dispatch (by minimizing generation costs or power losses or a combination of both) and voltage stability are often separate management issues. Similarly, frequency regulation is commonly performed by controlling real power, and voltage quality is managed by controlling reactive power generation or VAR compensation.

To expand on the above, power losses have been studied extensively in traditional power grids and also in various MGs involving renewable energy resources, controllable loads, and energy storage systems [9, 10, 11, 12]. The minimization of power losses is used to compute the optimal charging profile of plug-in hybrid electric vehicles (PHEV) in [13] . Overloading of lines and minimization of power losses are used as sensitivity factors to coordinate the charging profile of plug-in electric vehicles

(PEVs) in [14]. While the cooperative power exchange algorithm is used to minimize the total power loss in [15], the algorithm only reached near-optimal results. .The power loss minimization problems in these papers do not include multiple objectives such as balanced load distribution to generators/feeders or voltage profile management. [12] utilizes a control strategy that uses Particle Swarm Optimization (PSO) to solve the optimization problem of reducing power losses in hybrid energy storage system (HESS) and state of charge (SOC) balance by employing a centralized voltage controller that is used to sense the current demand and batteries' state of charge.

Furthermore, this work seeks distributed strategies to achieve global optimal solutions. MG Central Controllers (MGCC) manage all control and decision actions by central systems through the information exchange between the MGCC and the load controllers (LCs) that control groups of loads and microsource controllers (MCs) that control the storage devices [16].In contrast, droop control methods for standing-alone MGs are decentralized control techniques [17, 18, 19]. The frequency droop control of distributed energy resources (DERs) is used as a decentralized control strategy in MGs [17]. [18] used a decentralized optimization strategy to optimize the system's operation cost of DC microgrid which is achieved when the incremental cost of all distributed generators reach equality through a voltage droop scheme. A distributed control strategy that will regulate the output of multiple photovoltaic generators (PVs) in distribution networks is introduced to handle the numerous PV generation in MGs [19]. Voltage droop control methods have been used for resistive low-voltage networks [20, 21]. The conventional grid control concept is downscaled to the low volt-

age grid by implementing the conventional droop control strategy into the distributed energy resources (DERs) and the renewable energy sources (RESs) enhancing the stability and safety of the LV-grids [20]. A droop active power strategy for overvoltage protection in low voltage feeders is used to increase the installed PV capacity and energy yield, considering both cases of having the same and different droop coefficients [21]. [22] introduces a robust voltage management droop control strategy under disturbance scenarios taking into consideration the dynamics of the DC/DC converters. Unlike conventional droop control strategies that don't address the sudden drop in DC bus voltage level, [23] overcame that problem using droop based control strategy for voltage management that took into consideration the dynamics of the loads.

A classic optimal power flow method was adapted for dispatch power in MGs with DGs [24, 25]. New methods have been proposed, such as cooperative control schemes for fair power generation and sharing in MGs [19, 26] and voltage stability [27]. Distributed strategies are employed for economic dispatch and system efficiency in [28] and [29].In [26], a cooperative control scheme between the classical distributed optimization algorithm and the operation of multiagent systems is used to solve the problem of optimal energy exchange between the loads of the MG and the generation units. A distributed state estimation, used for condition monitoring such as fault detection by using an implementation of distributed Extended Kalman Filter and distributed Unscented Kalman Filter [27]. A cooperative robust control strategy of multi machine power system between an L_2 disturbance attenuation excitation controller for the generators and an adaptive L_2 disturbance attenuation excitation controller for

the superconducting magnetic energy storage (SMES) is used to enhance the system's stability [30]. A distributed adaptive droop control is used to optimize the microgrid's power distribution of the economic dispatch problem in [28]. The optimal solution is obtained through using a distributed hierarchical control that eliminates the need of centralized controllers .In [29], a dynamic consensus based distributed optimization strategy was used to optimize the efficiency of a droop controlled DC microgrid. The droop control is used for fair load allocation among the DC/DC converters. [29] offers higher expandability and flexibility compared to the centralized strategies since each local agent obtains the global information for its local controller's decision making. On the other hand, the consensus method was applied to power system load distribution in [31]. Global optimality under combined performance objectives has not been established in these methods except for [28]. On the other hand, [32] showcases a multi-objective optimization control strategy that uses multi-objective Genetic Algorithm which determines the system's design based on the objectives of network size, cost and availability of energy in a hybrid renewable energy system in a smart microgrid.

Finally, this work employs stochastic approximation (SA) algorithms for real-time recursive updating of control actions. Different methods have been used in the literature. In [33], by using a Lyapunov optimization technique, a long-term energy cost was minimized under uncertainties in electricity price, workload, renewable energy generation, and power outage state in MGs. Minimization of a combined criterion on power loss and voltage stability was employed for optimal DG placement in [34]. The

problem was solved by using dynamic programming in [34], and particle swarm optimization algorithms in [35, 36]. A meta-heuristic harmony search algorithm (HSA) was used in [37] to solve network reconfiguration problems by minimizing power losses and improving voltage profiles in distribution networks with distributed generators. Expanding on power loss reduction and voltage sag avoidance, [38] also included economical factors such as installation and maintenance costs.

1 Potential Contribution

The objective of using distributed strategies to achieve global optimal solutions together with the use of SA algorithms is new in this application area.

This work is a significant extension on the distributed control strategies that integrates three performance objectives in dual-source trolleybus systems [39, 40] by incorporating voltage profiles and dealing with more general DC MGs. Additionally, it also incorporates subsystem dynamics in the second part of the work. The reference [39] treated load sharing only without optimization. Line losses were added in [40] and the corresponding optimization problem was investigated.

The following aspects of this work are new: (1) The voltage profiles along load sharing and loss reduction are integrated into the control problem. (2) Due to couplings of network voltages and currents, inclusion of bus voltages adds certain constraints and creates complications in achieving global optimality by distributed strategies. This work employs a decoupling weighting to restore global optimality of our distributed algorithms. (3) Modified recursive and distributed algorithms are devel-

oped whose convergence properties are established. (4) The methodology is extended to include generators of different capacities, leading to a weighted consensus for load sharing. (5) The trade-off among conflicting objectives is studied and demonstrated. (6) The methodology is extended to include subsystem dynamics.

1 Dissertation Organization

This dissertation is structured as follows:

In Chapter 2, background information about microgrids and the different type of optimization techniques used in microgrids.

In Chapter 3, a distributed control strategy is developed to solve the multi-objective optimization problem in order to find the optimal feeder currents in a DC microgrid, a recursive algorithm that is capable of achieving the global optimal solution using only neighborhood communications. Multiple case studies were employed to evaluate the optimization strategy using the power supply system configurations of the Beijing Dual-Source Trolleybus System in [39] and a 14-DC bus system.

Chapter 4 extends on the work from chapter 3 by including subsystem dynamics in addition to optimal load sharing, loss reduction and voltage quality in optimization in DC microgrids. The local dynamics are realized by a state space model. Convergence analysis is conducted on the modified algorithm. DC-DC buck converter is used as the subsystem dynamic in the case studies that will be controlled using a PI controller. More case studies were introduced to evaluate the effect of the controller's dynamics, converter's dynamics and step size and sampling interval on the system behavior.

Chapter 5 highlights a conclusion drawn from the work in addition to providing some ideas that might be pursued for future work.

2   BACKGROUND

2   DC Microgrids

2.1.1   Definition Of Microgrids

First, general definitions of microgrids are needed. There are a lot of microgrid definitions presented by various reports from different research organizations all over the world. Some of those definitions of a microgrid are as follows:

The U. S. National Renewable energy laboratory (NREL) has provided the following definition of Microgrids in [41]:

"A microgrid is a group of interconnected loads and distributed energy resources that acts as a single controllable entity with respect to the grid. It can connect and disconnect from the grid to operate in grid-connected or island mode. Microgrids can improve customer reliability and resilience to grid disturbances."

The Congressional Research Service (CRS) presents a Microgrid definition in [42] as follows:

" A Microgrid is any small or local electric power system that is independent of the bulk electric power network. For example, it can be a combined heat and power system based on a natural gas combustion engine (which cogenerates electricity and hot water or steam from water used to cool the natural gas turbine), or diesel generators, renewable energy, or fuel cells. A Microgrid can be used to serve the electricity needs of data centers, colleges, hospitals, factories, military bases, or entire communities (i.e., "village power")."

From these definitions, a microgrid should include the following:

-A microgrid is an integration of microsources, storage units and controllable loads located in a local distribution grid.

- A microgrid can operate in grid-connected or disconnected modes.

The next section will briefly discuss the reasons why there is a shift toward microgrids.

2.1.2 Why Microgrids

There are benefits of using microgrids to the environment, and to utility operators and customers. In addition to the capability of operating in grid-connected and stand-alone modes, other benefits and advantages for using microgrids are development flexibility, increased power quality and efficiency.

Microgrids benefit from distributed generation, eliminating the constraints on high penetration which results in environmental benefits through the utilization of energy efficient generation resources. Thus, less fuel is combusted overall, resulting in lower greenhouse gas emissions [43]. Additionally, the integration of distributed energy resources increases reliability which may result to reduction in the cost of energy and reduction in power losses [44].

Microgrids can continuously power buildings and important facilities even if the surrounding areas are suffering from an outage. This feature of microgrids offers greater grid resilience from weather-related and cybersecurity issues compared to those grids without microgrids, which could suffer from outages [45].

For the purpose of the work, DC microgrids will be further discussed in the next subsections.

2.1.3 Configuration of DC Microgrids

A microgrid consists of energy resources, loads and management / coordination units and energy storage units. It is possible to integrate both renewable energy sources (e.g. photovoltaic, wind) and conventional sources (such as diesel fuel) in a microgrid. It also has to support main power networks. Conditioning and management Units allow voltage level adjustments, interactions with other units in the grid, and interaction with the loads. Examples of those units are DC/AC Inverters and DC/DC Converters [46].

By connecting all the sources and loads to the DC inks, DC microgrid is formed. The AC utility grid and the AC distributed generation units are connected via bidirectional DC/AC inverters. The PV units, energy storage units and DC loads are linked to the DC bus through DC/DC converters as shown in Fig. 1.
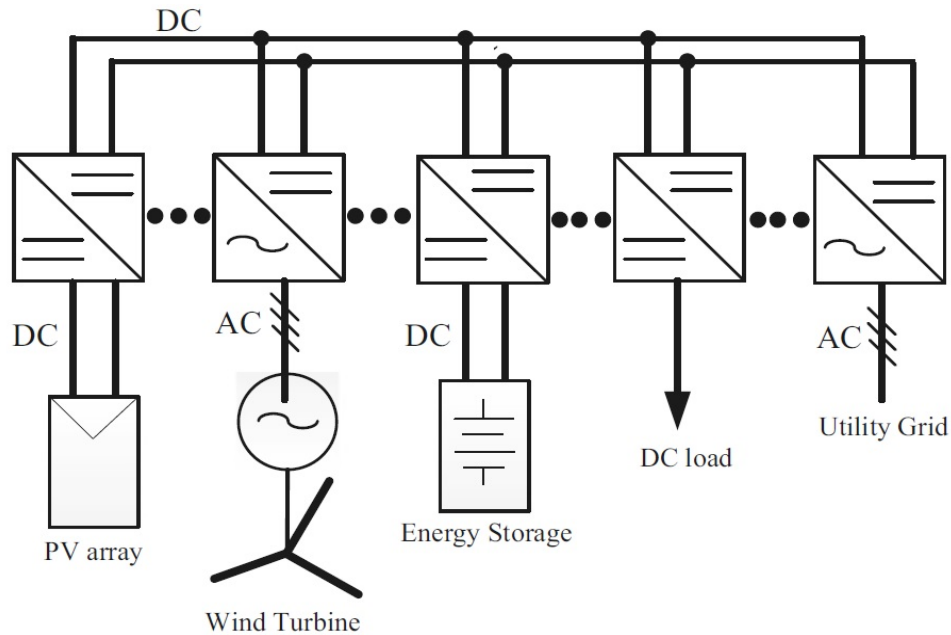
Figure 1: DC Microgrid [47].

2.1.4   Why DC Microgrids

There are advantages and reasons behind the increase of using DC microgrids over AC microgrids, some of which are as follow:

1. **Sources:** there is a resurgence in using DC because of the apparent increase in DC generation all over the world including solar power and fuel cells. Solar power is booming all over the world including the United States, which has experienced annual average growth of 68% in the last decade [48]. Another example would be Kamuthi Solar PV Power Plant India, which is the world's largest solar power plant with an installed capacity of 648 MW [49].

2. **Loads:** there is also a noticeable increase in DC loads. Most modern electronics and technologies (such as TVs and computers) require DC power. Data Centers, for example, require the use of DC power for their equipments such as servers, motors and batteries. DC data centers are more efficient than the AC ones [50].

3. **Distributed Energy:** a DC microgrid will enable distributed energy resources better than an AC microgrid. DC MG with distributed energy involved offers better conversion efficiency as well as better transmission/distribution efficiency [47].

Additionally, DC microgrids feature a reduction of AC-DC converters, power loss reduction and decentralization of the grid.

2 Optimization

A general definition of optimization in electric power systems is provided by the National Energy Technology Laboratory (NETL) from the Department of Energy [51], which is as follow:

"A broad set of interrelated decisions on obtaining, operating, and maintaining physical and human resources for electricity generation, transmission, and distribution that minimize the total cost of providing electric power to all classes of consumers, subject to engineering, market, and regulatory constraints"

Power System Optimization is aimed at improvements in more areas than cost. It is also aimed at improving the system's security, reliability, efficiency, friendless to the environment, economics and stability. Identifying the prime design variables is the first step to formulate an optimization problem. A design problem usually involves many design parameters. Other parameters that are not as important usually remain fixed or vary depending on the relation with the prime design variables. Choosing as few design variables as possible is an important rule when formulating an optimization problem[52].

There are two distinct types of optimization algorithms based on the method of operation[52]:

1. **Deterministic Algorithms:** referred to the optimization algorithms used to solve optimization problems whilst providing theoretical guarantees that the reported solution is indeed the global one [53].

2. **Stochastic Algorithms:** referred to the optimization algorithms and strategies used to solve optimization problems (minimizing or maximizing an objective function) when randomness is present. Other common names for the objective function are loss function, performance measure and fitness function. Usually, randomness enters the optimization problem through the cost function or the constraint set [54].

For a deterministic algorithm, in each executable step, there exists *at most one* way to proceed. If there is no way to proceed, the algorithm is terminated. Deterministic algorithms do not use randomized numbers in order to decide what to do or how to modify data, unlike randomized algorithms. Using the same inputs will always produce the same results when using deterministic algorithms [52].

Optimization algorithms are categorized based on the communication structure to the following [55]:

1. **Centralized Algorithms:** algorithms where a centralized entity is responsible for computational performance, receiving information from agents, and finally sends new commands accordingly.

2. **Decentralized Algorithms:** purely local algorithms without any sort of communication between agents.

3. **Distributed Algorithms:** algorithms where each agent communicate with its neighboring agents only while there is no centralized entity to give any commands.

Centralized optimization and control algorithms have been the prominent algorithms when it comes to electric power systems. Some of the important objectives of those algorithms are the optimal dispatch of power flow and scheduled load sharing [55]. The increased penetration of distributed energy resources (DERs) such as PV generation will lead to a potential augmenting of the centralized structure with distributed algorithms.

Distributed algorithms have several potential advantages over the centralized counterparts. The fact that the computing agents only share limited information to the neighboring agents could potentially improve the cybersecurity and reduce the expanse of communication infrastructure. Additionally, distributed algorithms could offer better robustness with respect to the failure of individual agents compared to the centralized approach [55].

2   The Consensus Problem

The consensus problem is a fundamental problem in control of multi-agent systems that requires agreement among a number of agents or processes on a single data value. To reach consensus, each agent begins in the undecided state and proposes a single value after communicating and exchanging values with other agents in each execution[56].

The requirements of a consensus algorithm are that the following conditions should hold for every execution [56]:

1. **Termination:** Every non-faulty process must eventually decide.

2. **Agreement:** The final decision of every non-faulty process must be identical.

3. **Validity:** If all non-faulty agents proposed the same value, then any correct process in the decided state has chosen that value.

If there is no failure, then reaching consensus is trivial. However, consensus in the presence of failures can be complex. The complexity differs and depends on the system's model and type of failure[57].

3   OPTIMAL POWER AND VOLTAGE MANAGEMENT

This chapter is going to cover the first part of the work which is to develop the distributed methodology without including the dynamics of any part of the system.

The chapter is organized into the following sections. Section 3.1 formulates the main problems. The main network configuration of the DC MGs under study is defined. A multi-objective global optimization problem is formulated and solved in Section 3.2. Section 3.3 presents a distributed optimization method that is shown to achieve the global optimal solution at steady state. The recursive algorithms and their convergence properties are established in Section 3.4. Finally, case studies are used to evaluate the methodology in section 3.5.

3   Problem Formulation

3.1.1   DC Microgrid Networks

Throughout this chapter and the consecutive chapters, the generic word "node"
is used to represent a physical feeder line, a bus, a supply line segment, etc. Suppose
that a DC power supply network contains r nodes. The nodes are connected by link
lines to form a physical MG. In addition, the nodes communicate with each other
via a communication system, forming an information (cyber) network. This creates a
cyber-physical system. Each node communicates only with its physically connected
neighbors is an assumption made throughout the work. Consequently, the physical
network and information network have the same network topology.

In this DC power network, the real-time supply current of the ith node is $I_i(t)$ (A),
its load is $L_i(t)$ (A), and the node voltage is $v_i(t)$ (V). We emphasize that the word
"supply" means the consolidated controllable current, which may be a combination
of synchronous generators with AC/DC converters, the manageable part of solar
systems, controllable loads, energy storage devices, etc. The "load" represents the
sum of all uncontrollable currents, such as fluctuations of wind or PV generators,
motors, buildings, EV charge stations, etc.

The network topology is represented by a directed graph G. For $(i,j) \in G$, the
current from the ith node to the jth node is $I_{ij}(t)$ (A), and the line resistance is R_{ij}
(Ω). Since $I_{ij} = -I_{ji}$, each line will have only one line current. Denote the node
current vector $u(t) = [I_1(t), \ldots, I_r(t)]^T$, where the superscript T means transpose.

Similarly, $v(t) = [v_1(t), \ldots, v_r(t)]^T$, $L(t) = [L_1(t), \ldots, L_r(t)]^T$. By specifying a given order of the links, y is the column vector of the link currents, $R = \text{diag}[R_{ij}]$ is the link resistance matrix. The supply line of the ith node has rated current γ_i. Define the node capacity matrix $\Gamma = \text{diag}[1/\gamma_i]$ and $\gamma = [\gamma_1, \ldots, \gamma_r]^T$.

In this work, it is assumed that the DC MG is connected (every node has a path to any other node); and there are no loops (loops in DC current-supply networks will cause non-uniqueness in determining the currents in the MG and hence are not permitted). Under these conditions, the number of the links satisfies $l_s = r - 1$. Seeking distributed control strategies and impose the following assumptions is sought to make the control system scalable, reliable, and simple.

Assumption 1 (1) Each node knows its own state and parameters. (2) Each node knows the link current and link resistance that is connected to it. (3) Each node knows its neighbor's rated capacity, but must estimate its neighbor's supply current with possible errors.

Example 1 To illustrate these concepts, consider the 6-node DC MG in Fig. 2, which, for convenience of case studies and comparison, is the same topology used in [39].
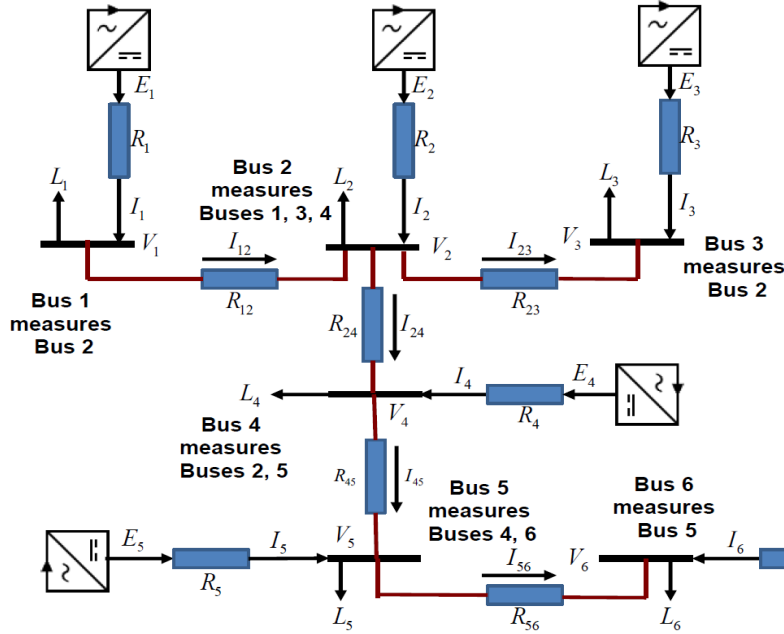
Figure 2: A DC microgrid with 6 feeders and 5 links.

Note that the MG and information network are identical: The node communicates only with its physically connected neighbors. For this MG, $G = \{(1,2),(2,3),(2,4),(4,5),(5,6)\}$ and $l_s = 5$, $y = [I_{12}(t), I_{23}(t), I_{24}(t), I_{45}(t), I_{56}(t)]^T$, $R = \text{diag}[R_{12}, R_{23}, R_{24}, R_{45}, R_{56}]$.

3.1.2 Design Objectives

Consider the following three control objectives.

1. **Fair Allocation of Loads to Generators.**

   In a networked system, multiple generators/feeders collectively support the loads on different nodes. Fair load sharing proportional to each generator's capacity can alleviate bus overload, reduce cost in generations, and avoid unnecessary tripping of protection circuits.

2. **Reduction of Line Power Loss.**

While allocating loads to different generators alleviates overload issues, transportation of currents among different buses introduces line power loss. A suitable control strategy needs to consider the tradeoff between load sharing and line loss reduction.

3. **Maintaining Desirable Voltage Profiles.**

   Allocating load currents to different generators has an unintended consequence on voltage profiles throughout the entire network. To guarantee power quality to the loads, the bus voltages must be managed to be close to their rated values.

To establish rigorous theoretical results on global optimality of the distributed strategies, to derive convergent algorithms, and to prove convergence under noisy observations, control objectives in the performance indices were purposely included, rather than imposing hard limits on them. For example, one may elect to impose hard bounds on node voltages as inequality constraints, rather than a performance term to be reduced; or designate link current limits that will ensure safety and implicitly limit line power loss.

Introducing such nonlinear inequality constraints in the optimization problems is common in practice. However, analytic or closed-form solutions to such problems remain unknown, and numerical solutions must be sought Furthermore, at present, it is not clear if distributed strategies can achieve the global optima under such problem formulations.

Obviously, these three objectives are in conflict with each other. For example, no

power sharing will avoid line losses completely, but lead to the worst-case scenario of bus overload. In this work, a multi-objective control will be formulated and its distributed optimal solutions are sought.

3   Multi-Objective Global Optimization

In a DC microgrid with r nodes, the node current vector u, link current vector y, and the load vector L are related by Kirchhoff's Current Law (KCL)

$$u = My + L \tag{3.1}$$

where M is an $r \times (r-1)$ network matrix whose rows are elementary vectors such that if the lth element of y flows into (or out) the jth node, then the value at (j, l)th position is -1 (or 1).

It is easy to verify that each column of M has exactly one -1 and one 1, representing the fact that each link current is from one node to another node, and $M^T \mathbb{1} = 0$, where $\mathbb{1}$ is the column vector of all 1s. M is full column rank, indicating that the link currents can be uniquely determined from the node currents and loads via

$$y = (M^T M)^{-1} M^T (u - L). \tag{3.2}$$

The node voltages are constrained by $r - 1$ equalities from the link currents, such

as $v_1 - v_2 = R_{12}I_{12}$. This can be written as

$$M^T v = Ry, \tag{3.3}$$

where R is the link resistance matrix.

Since there are only $r - 1$ equality constraints in (3.3), one degree of freedom on the node voltages remains. Imposing an extra condition will be generically expressed as an equality constraint

$$\zeta_o v = v_{ref}, \text{ with } \zeta_o \mathbb{1} = 1. \tag{3.4}$$

For example, if one bus, say node 1, is designated as a reference bus whose voltage is independently controlled to be v_{ref}, then $\zeta_o = [1, 0, \ldots, 0]$. If the average value of all bus voltages is controlled to be v_{ref}, then $\zeta_o = [1/r, \ldots, 1/r]$.

This requirement will be maintained in distributed algorithms presented in the subsequent sections. By adding (3.4) to (3.3), we have

$$H_0 v = R_0 y + W v_{ref} \tag{3.5}$$

where

$$H_0 = \begin{bmatrix} M^T \\ \zeta_o \end{bmatrix}, R_0 = \begin{bmatrix} R \\ 0, \ldots, 0 \end{bmatrix}, W = \begin{bmatrix} [0, \ldots, 0]^T \\ 1 \end{bmatrix}.$$

Under the condition that the DC MG is connected, H_0 is full rank. Then v can

be written as a function of y

$$v = H_0^{-1} R_0 y + H_0^{-1} W v_{ref}. \tag{3.6}$$

Moreover, from the expression of H_0, it is easy to deduce that

$$H_0 \mathbb{1} = \begin{bmatrix} 0 \\ \vdots \\ 0 \\ 1 \end{bmatrix} = W,$$

which implies that $H_0^{-1} W = \mathbb{1}$. Furthermore, $H_0^{-1} R_0$ can be expressed as

$$H_0^{-1} R_0 = H_0^{-1} \begin{bmatrix} R \\ 0 \end{bmatrix} = H_0^{-1} \begin{bmatrix} I \\ 0 \end{bmatrix} R = QR$$

in which $Q = H_0^{-1} \begin{bmatrix} I \\ 0 \end{bmatrix}$ depends only on the network topology, but not on the network parameters R_{ij}. These lead to

$$v = QRy + v_{ref} \mathbb{1}. \tag{3.7}$$

It can be verified that Q has rank $r - 1$; and hence $Q^T Q$ is full rank.

Example 2 *For the MG in Fig. 2 and $\zeta_o = [1/6, \ldots, 1/6]$, the corresponding network*

matrices are

$$M = \begin{bmatrix} 1 & 0 & 0 & 0 & 0 \\ -1 & 1 & 1 & 0 & 0 \\ 0 & -1 & 0 & 0 & 0 \\ 0 & 0 & -1 & 1 & 0 \\ 0 & 0 & 0 & -1 & 1 \\ 0 & 0 & 0 & 0 & -1 \end{bmatrix},$$

$$H_0 = \begin{bmatrix} 1 & -1 & 0 & 0 & 0 & 0 \\ 0 & 1 & -1 & 0 & 0 & 0 \\ 0 & 1 & 0 & -1 & 0 & 0 \\ 0 & 0 & 0 & 1 & -1 & 0 \\ 0 & 0 & 0 & 0 & 1 & -1 \\ 1/6 & 1/6 & 1/6 & 1/6 & 1/6 & 1/6 \end{bmatrix},$$

$$Q = \begin{bmatrix} 5/6 & -1/6 & -1/6 & -1/6 & -1/6 \\ -1/6 & 5/6 & -1/6 & -1/6 & -1/6 \\ -1/6 & -1/6 & 5/6 & -1/6 & -1/6 \\ -1/6 & -1/6 & -1/6 & 5/6 & -1/6 \\ -1/6 & -1/6 & -1/6 & -1/6 & 5/6 \\ -1/6 & -1/6 & -1/6 & -1/6 & -1/6 \end{bmatrix}.$$

The goal of power management in this networked system consists of three objectives: (a) Balance the node currents such that $u(t) - \beta\gamma$ is small, where β is a

constant. (b) Reduce line power losses $y^T R y$. (c) Maintain the bus voltages to be close to the rated value v_{ref}, namely $v - v_{ref}\mathbb{1}$ should be small.

The desired load sharing is $u(t) = \beta\gamma$. By the current balance, $L(t)^T\mathbb{1} = u^T\mathbb{1} = \beta\gamma^T\mathbb{1}$. Therefore, $\beta = L(t)^T\mathbb{1}/\gamma^T\mathbb{1}$, namely the used (total) capacity in percentage. Since β involves all the loads, it is a global variable and is not available to distributed controllers.

A multi-objective performance index is introduced here to define a tradeoff among these three objectives. Define a weighting matrix $\Phi = Q(Q^T Q)^{-1}(Q^T Q)^{-1}Q^T$, and

$$J = \tfrac{1}{2}[a(u - \beta\gamma)^T\Gamma(u - \beta\gamma) + by^T R y$$
$$+ c(v - v_{ref}\mathbb{1})^T\Phi(v - v_{ref}\mathbb{1})],$$

(3.8)

subject to the constraints (3.1) and (3.7). Here a, b, c with $a + b + c = 1$ are scalar non-negative weighting coefficients that define a trade-off among the three objectives. The weighting matrices $\Gamma = \mathrm{diag}[1/\gamma_i]$ and Φ serve the purpose of decoupling and scaling so that distributed strategies can be used.

Denote $\Gamma^{1/2} = \mathrm{diag}[1/\sqrt{\gamma_i}]$, $M_0 = \Gamma^{1/2}M$, and $L_0 = \Gamma^{1/2}L$. Under the relations (3.1) and (3.7), the performance index (3.8) becomes

$$
\begin{aligned}
J(y) &= \frac{1}{2}[a(\Gamma^{1/2}(My + L) - \beta\Gamma^{1/2}\gamma)^T(\Gamma^{1/2}(My + L) - \beta\Gamma^{1/2}\gamma) \\
&\quad + by^T R y + cy^T R Q^T\Phi Q R y] \\
&= \frac{1}{2}[a(M_0 y + L_0 - \beta\Gamma^{1/2}\gamma)^T(M_0 y + L_0 - \beta\Gamma^{1/2}\gamma) \\
&\quad + by^T R y + cy^T R Q^T\Phi Q R y]
\end{aligned}
$$

$$= \frac{1}{2}[a(M_0 y + L_0 - \beta\Gamma^{1/2}\gamma)^T(M_0 y + L_0 - \beta\Gamma^{1/2}\gamma)$$

$$+ by^T Ry + cy^T R^2 y].$$

Consequently, the link current vector y becomes naturally the control variable.

The goal of optimization aims to minimize the performance index

$$\min_y J(y). \tag{3.9}$$

Theorem 1 *The global optimal solution to* (3.9) *is*

$$y^* = -[aM_0^T M_0 + bR + cR^2]^{-1} aM_0^T L_0. \tag{3.10}$$

Proof: To solve the optimization problem, we calculate the stationary point

$$\frac{\partial J(y)}{\partial y} = aM_0^T(M_0 y + L_0 - \beta\Gamma^{1/2}\gamma) + bRy + cR^2 y$$

$$= [aM_0^T M_0 + bR + cR^2]y + aM_0^T(L_0 - \beta\Gamma^{1/2}\gamma)$$

$$= [aM_0^T M_0 + bR + cR^2]y + aM_0^T L_0$$

$$= 0.$$

Here, the fact

$$M_0^T \Gamma^{1/2}\gamma = M^T \Gamma\gamma = M^T \mathbb{1} = 0$$

is used in the derivation. Hence, the optimal link current vector y^* is

$$y^* = -[aM_0^T M_0 + bR + cR^2]^{-1} aM_0^T L_0.$$

Furthermore, the Hessian matrix is

$$aM_0^T M_0 + bR + cR^2.$$

Since $M_0^T M_0 > 0$, $R > 0$, $R^2 > 0$, this matrix is positive definite as long as one of the coefficients is positive. This implies that y^* is indeed the minimum point. $\square$

Remark 1 While the global optimal solution can be calculated without any iteration, it requires a central controller and global information on the network parameters and loads on all buses. Consequently, it needs intensive communication resources. Furthermore, when the network scales by expanding and shrinking, the network parameter matrix R, topology matrix M, and local loads L must be updated at the central controller. In this sense, it is not friendly to network scaling.

3   Distributed Optimization

The main goal here is to develop a distributed control that does not require a central controller or global exchange of information, but can still achieve the global optimal solution (3.10). In addition to Assumption 1, a cooperative and consistent decision environment is assumed: a decision on the link current I_{ij} (the local control variable) is shared by node i and node j. As a result, a distributed control strategy will be an optimization over the link current I_{ij} individually for each link. In other words, in deciding I_{ij}, a local performance index needs to be used that involves only $I_i, v_i,\ I_j, v_j,$ and R_{ij}.

The main challenge is to determine the local performance index so that the global optimal solution (3.10) can be achieved without global information exchange.

For each link $(i, j) \in G$, its local objective function is defined as

$$
\begin{aligned}
J_{ij} &= \tfrac{1}{2}[\tfrac{a}{2}\left(\tfrac{I_i}{\gamma_i} - \tfrac{I_j}{\gamma_j}\right)^2 + bR_{ij}I_{ij}^2 + c(v_i - v_j)^2] \\
&= \tfrac{1}{2}[\tfrac{a}{2}\left(\tfrac{I_i}{\gamma_i} - \tfrac{I_j}{\gamma_j}\right)^2 + bR_{ij}I_{ij}^2 + cR_{ij}^2I_{ij}^2].
\end{aligned}
\tag{3.11}
$$

Theorem 2 *The local optimal solutions to* (3.11) *are identical to the global optimal solution* (3.10).

Remark 2 Each link current I_{ij} is a player who makes its decision on the basis of the local performance index J_{ij}. This may be viewed as a cooperative game of $r - 1$ players with network-constrained partial observations. Theorem 2 states that the

equilibrium of the game exists, is unique, and equals the global solution (3.10).

Proof: The optimal I_{ij} can be derived locally from the local optimality condition

$$
\begin{aligned}
\frac{\partial J_{ij}}{\partial I_{ij}} &= \frac{a}{2}\left(\frac{I_i}{\gamma_i} - \frac{I_j}{\gamma_j}\right)\left(\frac{\partial I_i}{\partial I_{ij}} - \frac{\partial I_j}{\partial I_{ij}}\right) + bR_{ij}I_{ij} + cR_{ij}^2 I_{ij} \\
&= a\left(\frac{I_i}{\gamma_i} - \frac{I_j}{\gamma_j}\right) + bR_{ij}I_{ij} + cR_{ij}^2 I_{ij} \\
&= 0,
\end{aligned}
$$

where the facts $\frac{\partial I_i}{\partial I_{ij}} = 1$ and $\frac{\partial I_j}{\partial I_{ij}} = -1$ have been applied.

Since

$$
\frac{\partial^2 J_{ij}}{\partial I_{ij}^2} = a\left(\frac{1}{\gamma_i} + \frac{1}{\gamma_j}\right) + bR_{ij} + cR_{ij}^2 > 0,
$$

this is indeed the local minimum point.

By considering all the links and expressing them in matrix form, the local optimality condition becomes

$$
aM^T\Gamma u + bRy + cR^2 y = 0. \tag{3.12}
$$

By using (3.1), $M^T\Gamma M = M_0^T M_0$, and $M^T\Gamma L = M_0^T L_0$, we have

$$
aM^T\Gamma(My + L) + bRy + cR^2 y = 0,
$$

or

$$
[aM_0^T M_0 + bR + cR^2]y + aM_0^T L_0 = 0,
$$

which is identical to (3.10). □

Although Theorem 2 establishes an information-theoretical conclusion that the distributed information is sufficient for obtaining the global optimal solution, the local optimal solutions cannot be achieved simultaneously in one step since the node currents are affected by all local controllers at each step and hence are not optimal in transient. A recursive algorithm will be introduced in the next section to resolve this issue.

3 Recursive Algorithms and Convergence Properties

This section introduces a recursive algorithm that is capable of achieving the global optimal solution (3.10) using only neighborhood communications.

A small time interval τ is selected to update the control actions at $t = n\tau$, $n = 1, 2, \ldots$ At the nth control step, the node currents are $u_n = [I_n^1, \ldots, I_n^r]^T$, the load currents $L_n = [L_n^1, \ldots, L_n^r]^T$, and link currents are $y_n = (M^T M)^{-1} M(u_n - L_n)$.

We design the following algorithm

$$u_{n+1} = u_n - \mu_n M\Pi[aM^T\Gamma u_n + bRy_n + cR^2 y_n - ad_n], \tag{3.13}$$

where $\{d_n\}$ is a sequence of observation noise vectors, $\{\mu_n\}$ is a sequence of step sizes satisfying $\mu_n \geq 0$, $\mu_n \to 0$ as $n \to \infty$, and $\sum_{k=1}^n \mu_k \to \infty$ as $n \to \infty$, $\Pi = \mathrm{diag}[g_{ij}]$ is the $(r-1) \times (r-1)$ diagonal matrix of the same order as R, $g_{ij} > 0$ is the link specific gain to allow different feedback gains on different links.

3.4.1 Algorithm Derivations

By (3.1), the link currents can be expressed as

$$
\begin{aligned}
y_n &= (M^T M)^{-1} M^T (u_n - L) \\
&= (M^T M)^{-1} M^T u_n - (M^T M)^{-1} M^T L.
\end{aligned}
\tag{3.14}
$$

Updating u_n in each step is defined by ξ_n

$$u_{n+1} = u_n + \xi_n, \tag{3.15}$$

where the ith component of ξ_n is determined by all link control variables λ_n^{ij} from node i to node j:

$$\xi_n^i = -\sum_{j:(i,j)\in G} \lambda_n^{ij} + \sum_{j:(j,i)\in G} \lambda_n^{ji} \tag{3.16}$$

The link control λ_n^{ij} depends on the available local information, and is arranged as a vector Λ of the same order as y. It is easy to verify that

$$\xi_n = -M\Lambda$$

The network must satisfy the conditions $\sum_{i=1}^r \xi_n^i = 0$ to ensure the physical condition that the total supply-side current is equal to the total load-side current

$$\sum_{i=1}^r u_n^i = \sum_{i=1}^r L_n^i.$$

A link $(i,j) \in G$ entails an estimate $\widehat{I}_n^j(i)$ of $I_n^j(i)$ by node i with observation noise $d_n^j(i)$.

$$\widehat{I}_n^j(i) = I_n^j + d_n^j(i). \tag{3.17}$$

Let η_n and d_n be the $(r-1)$-dimensional vectors that contain all $\widehat{I}_n^j(i)$ and $d_n^j(i)$, respectively, arranged in the same order as y. Then (3.17) becomes $\eta_n = H_1 u_n + d_n$,

where H_1 is an $(r-1) \times r$ matrix whose rows are elementary vectors such that if the lth element of η_n is $\widehat{I}_n^j(i)$, then the lth row in H_1 is the row vector of all zeros except for a 1 in the jth position. For the DC MG in Fig. 2,

$$H_1 = \begin{bmatrix} 0 & 1 & 0 & 0 & 0 & 0 \\ 0 & 0 & 1 & 0 & 0 & 0 \\ 0 & 0 & 0 & 1 & 0 & 0 \\ 0 & 0 & 0 & 0 & 1 & 0 \\ 0 & 0 & 0 & 0 & 0 & 1 \end{bmatrix}.$$

Based on the available information, the local objective function (3.11) becomes

$$\widehat{J}_{ij} = \frac{1}{2}[\frac{a}{2}\left(\frac{I_n^i}{\gamma_i} - \frac{\widehat{I}_n^j(i)}{\gamma_j}\right)^2 + bR_{ij}(I_n^{ij})^2 + cR_{ij}^2(I_n^{ij})^2], \tag{3.18}$$

whose gradient is

$$\begin{aligned}
\delta_n^{ij} &= \frac{\partial \widehat{J}_{ij}}{\partial I_n^{ij}} \\
&= \frac{a}{2}\left(\frac{I_n^i}{\gamma_i} - \frac{\widehat{I}_n^j(i)}{\gamma_j}\right)\left(\frac{1}{\gamma_i}\frac{\partial I_n^i}{\partial I_n^{ij}} - \frac{1}{\gamma_j}\frac{\partial \widehat{I}_n^j(i)}{\partial I_n^{ij}}\right) \\
&\quad + bR_{ij}I_n^{ij} + cR_{ij}^2 I_n^{ij} \\
&= a\left(\frac{I_n^i}{\gamma_i} - \frac{\widehat{I}_n^j(i)}{\gamma_j}\right)\left(\frac{I_n^i}{\gamma_i} + \frac{I_n^i}{\gamma_j}\right) + bR_{ij}I_n^{ij} + cR_{ij}^2 I_n^{ij}
\end{aligned}$$

or compactly as a vector

$$\delta_n = a(H_2\Gamma u_n - \eta_n) + bRy_n + cR^2 y_n,$$

where H_2 is an $(r-1) \times r$ matrix whose rows are elementary vectors such that if the lth element of η_n is $\widehat{I}_n^j(i)$, then the lth row in H_2 is the row vector of all zeros except for a 1 in the ith position. For the DC MG in Fig. 2,

$$H_2 = \begin{bmatrix} 1 & 0 & 0 & 0 & 0 & 0 \\ 0 & 1 & 0 & 0 & 0 & 0 \\ 0 & 1 & 0 & 0 & 0 & 0 \\ 0 & 0 & 0 & 1 & 0 & 0 \\ 0 & 0 & 0 & 0 & 1 & 0 \end{bmatrix}.$$

The local link control action is a gain feedback $\lambda_n^{ij} = \mu_n g_{ij} \delta_n^{ij}$, where $g_{ij} > 0$ is the link specific gain to allow different feedback gains on different links, and μ_n is a step size to be specified later. Let $\Pi = \mathrm{diag}[g_{ij}]$ be the $(r-1) \times (r-1)$ diagonal matrix of the same order as R. Note that $M^T = H_2 - H_1$. As a result,

$$\Lambda = \mu_n \Pi [a(H_2 \Gamma u_n - \eta_n) + bR y_n + cR^2 y_n]$$

$$= \mu_n \Pi [a(H_2 \Gamma u_n - H_1 \Gamma u_n - d_n) + bR y_n + cR^2 y_n]$$

$$= \mu_n \Pi [aM^T \Gamma u_n + bR y_n + cR^2 y_n - ad_n].$$

Thus, the node control becomes

$$\xi_n = -M \mu_n \Pi [aM^T \Gamma u_n + bR y_n + cR^2 y_n - ad_n].$$

It follows that

$$u_{n+1} = u_n - \mu_n M\Pi[aM^T\Gamma u_n + bRy_n + cR^2 y_n - ad_n],$$

which is (3.13).

3.4.2 Convergence Analysis of Algorithm

Note that (3.13) is a stochastic approximation algorithm [58], in which $\{\mu_n\}$ is a sequence of the step sizes as given in (3.13). To proceed, the following assumed condition holds.

Assumption 2 *The noise $\{d_n\}$ is a stationary ϕ-mixing sequence such that $Ed_n = 0$, $Ed_n^{2+\Delta} < \infty$ for some $\Delta > 0$, and that the mixing measure $\tilde{\phi}_n$ satisfies*

$$\sum_{n=0}^{\infty} \tilde{\phi}_n^{\frac{\Delta}{(1+\Delta)}} < \infty,$$

where E is the expectation, and P is the probability.

The ϕ-mixing sequence defined in Assumption 2 indicates that the remote past and distant future are asymptotically independent. It is noted that the mixing condition on the noise is much more realistic and allows the observation noises to be correlated.

To prove the convergence, connect the discrete iteration with a continuous-time system by defining $t_n = \sum_{k=0}^{n-1} \mu_k$. Let $u^0(t)$ be a piecewise constant interpolation of u_n on the interval $[t_n, t_{n+1})$ and $u^n(t) = u^0(t+t_n)$ be its shifted sequence. Denoting the

"inverse" by $m(t) = \max\{n : t_n \le t\}$. By the relationship $y = (M^T M)^{-1} M^T (u - L)$

in (4.2), also $y^n(t) = (M^T M)^{-1} M^T \Gamma(u^n(t) - L)$.

Then it can be shown that the sequence $\{u^n(\cdot)\}$ (and $\{y^n(\cdot)\}$) is in an appropriate

function space that is uniformly bounded and equi-continuous in the extended sense

(defined in [59]). By using the extended version of the Arzela-Ascoli Theorem (see

also [59]), it can be shown that $\{u^n(\cdot)\}$ (and $\{y^n(\cdot)\}$) has a convergent subsequence

with limit $u(\cdot)$ (and $y(\cdot)$) such that $u(\cdot)$ satisfies the ordinary differential equation

$$\dot{u} = -M\Pi[aM^T \Gamma u + bRy + cR^2 y], \tag{3.19}$$

and

$$\dot{y} = (M^T M)^{-1} M^T \Gamma \dot{u}$$

$$= (M^T M)^{-1} M^T (-M\Pi[a(M)^T \Gamma u + bRy + cR^2 y])$$

$$= -\Pi[aM^T \Gamma u + bRy + cR^2 y]$$

$$= -\Pi[(aM_0^T M_0 + bR + cR^2)y + aM_0^T L_0]$$

The equilibrium point of the ODE for y is the solution to

$$0 = \Pi[(aM_0^T M_0 + bR + cR^2)y + aM_0^T L_0].$$

Since Π is full rank,

$$y^* = -[a(M_0^T M_0 + bR + cR^2]^{-1} aM_0^T L_0 \tag{3.20}$$

which is identical to the global optimal solution in (3.10).

Consider the error between the global optimal solution and the local link current

$$e = y - y^* \qquad (3.21)$$

where y^* is given by (3.20). In view of (3.21),

$$
\begin{aligned}
\dot{e} &= -\Pi[aM_0^T M_0 + bR + cR^2)y + aM_0^T L_0] \\
&= -\Pi[aM_0^T M_0 + bR + cR^2)(e + y) + aM_0^T L_0] \qquad (3.22) \\
&= -\Pi[(aM_0^T M_0 + bR + cR^2)]e
\end{aligned}
$$

knowing that $(aM_0^T M_0 + bR + cR^2)y + aM_0^T L_0 = 0$. This system has the unique equilibrium point $e = 0$ and is stable.

Theorem 3 *Under Assumption 2, $y^n(\cdot + q_n) \to y^*$ with probability 1 as $n \to \infty$, where $q_n \to \infty$ as $n \to \infty$ and y^* is the stable stationary point of the ODE (3.22).*

Proof:

This is a sketch highlighting the main ideas of the proof. More details can be found in [59].

First, the convergence of the global optimal solution u^* follows the convergence standard arguments in [59]. The convergence of the distributed solution u follows the convergence of the global optimal solution u^* under the condition that the Limit ODE is asymptotically stable.

To show stability, note that Π is diagonal and positive definite, and can be written as $\Pi = \psi^2$ with $\psi = diag[\sqrt{gij}]$.

Now, the eigenvalues

$$\Pi[(aM_0^T M_0 + bR + cR^2)] = \psi\psi[(aM_0^T M_0 + bR + cR^2)]$$

are exactly the same as the eigenvalues of $\psi[(aM_0^T M_0 + bR + cR^2)]\psi$ which are all real and positive. From the above as a result, $\Pi[(aM_0^T M_0 + bR + cR^2)]$ is asymptotically stable and is the stationary point of the ODE [40]. □

Note that the consequence of the above theorem is that the sequence of iterates converges to the desired optimumthe stationary point.

3 Case Studies

3.5.1 Trolleybus Systems

Trolleybus systems will be the first example of microgrids that the methodology will be applied on. In the literature, power losses in addition to other individual performance considerations,economic dispatch, frequency regulation using real power control, and voltage management using VAR compensator, have been studied in various MGs involving renewable energy resources, controllable loads, electric vehicles (EVs), and energy storage systems [13, 14, 15, 9].

For methodology evaluation, the power supply system configurations of the Beijing Dual-Source Trolleybus System in [39] are used for simulation case studies on the new power management methods introduced in this work. Here, only some features that are necessary for our model construction are summarized.
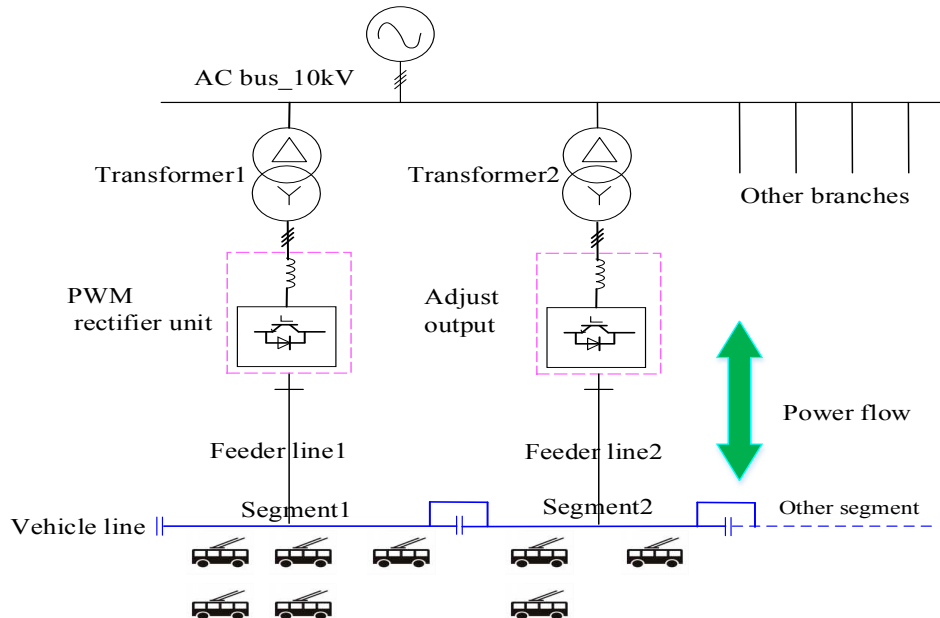

Figure 3: Diagram of the trolleybus power supply network.

Fig. 3 is re-produced from [39, 40].

Consider the trolleybus system in Fig.2. The system consists of six segments and five communication links $G = \{(1, 2), (2, 3), (2, 4), (4, 5), (5, 6)\}$. The feeders' initial currents are $I(0) = [713, 811, 960, 844, 887, 823]^T$ (A), the (constant) load vector is $L(t) = [681, 783, 1009, 842, 921, 803]^T$, the link currents are labeled as $y(t) = [I_{12}(t), I_{23}(t), I_{24}(t), I_{45}(t), I_{56}(t)]^T$. The line resistances are calculated based on the station supply radii with values $R = \text{diag}[R_{12}, R_{23}, R_{24}, R_{45}, R_{56}] = \text{diag}[0.4, 0.38, 0.34, 0.31, 0.36]$ (Ω). The rated bus voltage is 650 (V).

The typical voltage tolerance bounds in case studies are within (10%) tolerance. Note that in such an optimization problem, if the voltages and currents are only required to be within the given bounds, one may formulate it as a constrained optimization problem, without including the voltage term in the performance index. In our problem, the voltages are not only required to be in the range, but also to be close to v_{ref} .

3.5.2   Optimality

We start with an evaluation of the distributed stochastic approximation algorithm (3.13) in terms of its ability to achieve the global optimal solution asymptotically.

Suppose that the weighting coefficients are $a = 0.3$, $b = 0.2$ and $c = 0.5$ and the step size is selected as $\mu_n = \frac{1}{n^v}$ with $0.5 < v < 1$. Link observation noises are i.i.d. sequences of Gaussian random variables of mean zero and variance 6.

Fig. 4 shows the simulation results. Subplot (a) shows that the feeders' currents
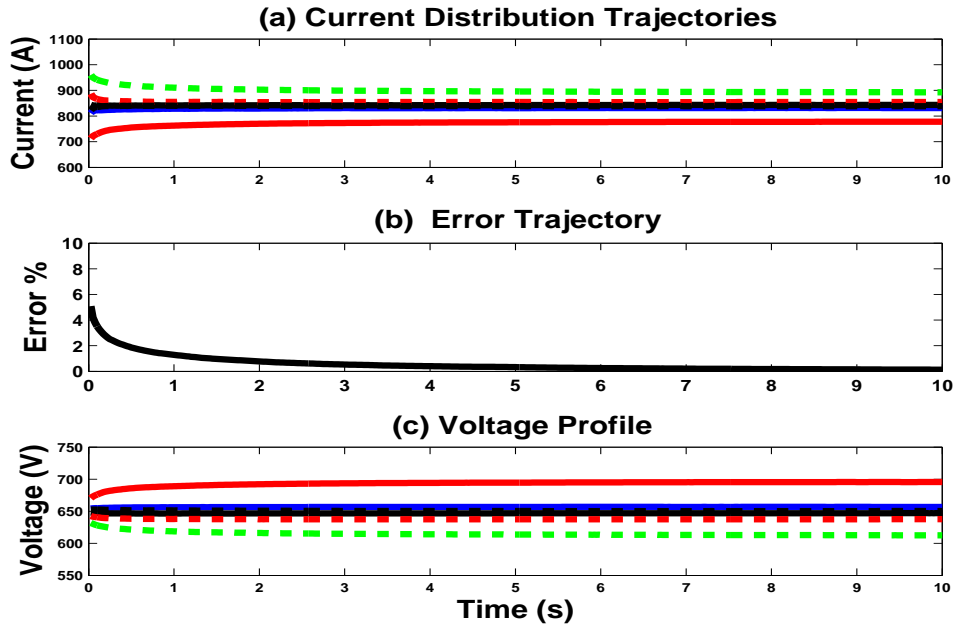
Figure 4: Feeder currents, optimality error trajectories, and voltage profiles under $a = 0.3$, $b = 0.2$ and $c = 0.5$

converge to their final values. Subplot (b) is the error trajectory of the differences between the performance levels that are achieved by the distributed recursive algorithm and the global optimum. Subplot (c) shows the voltage profile. The errors converge to zero, indicating asymptotic global optimality of the algorithm.

Under the selected weighting coefficients $a = 0.3$, $b = 0.2$ and $c = 0.5$, the total link power loss is 9.926 kW. In comparison, without optimization, the initial link power loss is 22.7 kW. Table 1 compares the optimal feeder currents using the recursive distributed algorithm and those from the global optimal solution.

Table 1: Optimality of Distributed Control

Current	I_1	I_2	I_3	I_4	I_5	I_6
Distributed Optimization (Local, $n = 400$) Amps	777.4	831.6	892.3	843.4	854.4	838.8
Global Optimization, Amps	779.4	831.8	890.4	843.8	854.9	838.7

It is apparent that the distributed optimization can reach asymptotically the global optima with errors less than 1%, which stem from observation noises.

3.5.3 Voltage Profiles

We now investigate voltage profiles. One important objective for the trolleybus systems is to maintain bus voltages within a small tolerance of their rated values.

If the weighting coefficients $a = 0.3$, $b = 0.2$ and $c = 0.5$ were to be used as before, Fig. 4 Subplot (c) shows that V_1 and V_2 deviate from the rated 650 (V) significantly. To improve the voltage profile while still allowing the nodes to support other neighboring nodes, the weighting coefficients can be tuned.

To have an acceptable voltage profile while still allowing the nodes to support other neighboring nodes, the weighting coefficients should be carefully tuned according to practical conditions of the network. For instance, to reduce voltage deviations in the original case study. Now, increase the weighting on c by using $a = 0.1$, $b = 0.3$ and $c = 0.6$. The results are shown in Fig. 5. The voltage profiles have been improved significantly.

Next, let $c = 1$ (this is a strategy of voltage management only). Intuitively, this should create a uniform voltage value as the optimal solution. This is indeed the case as illustrated in Fig. 6. The currents are now distributed solely according to the local loads. We can see that by supporting only the local loads, the line currents are equal to 0, thus the link power losses are also 0, which is the global optimal solution for this specific case.
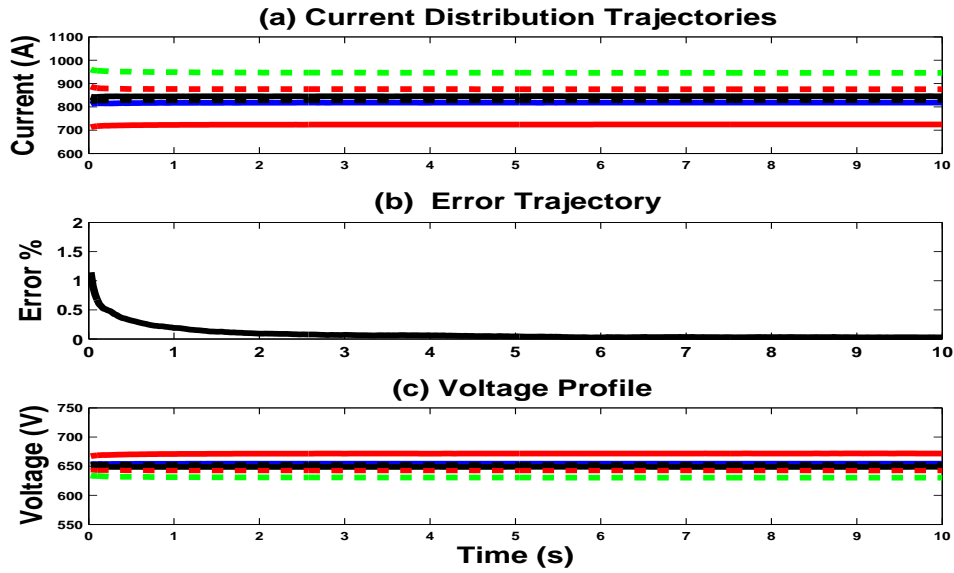
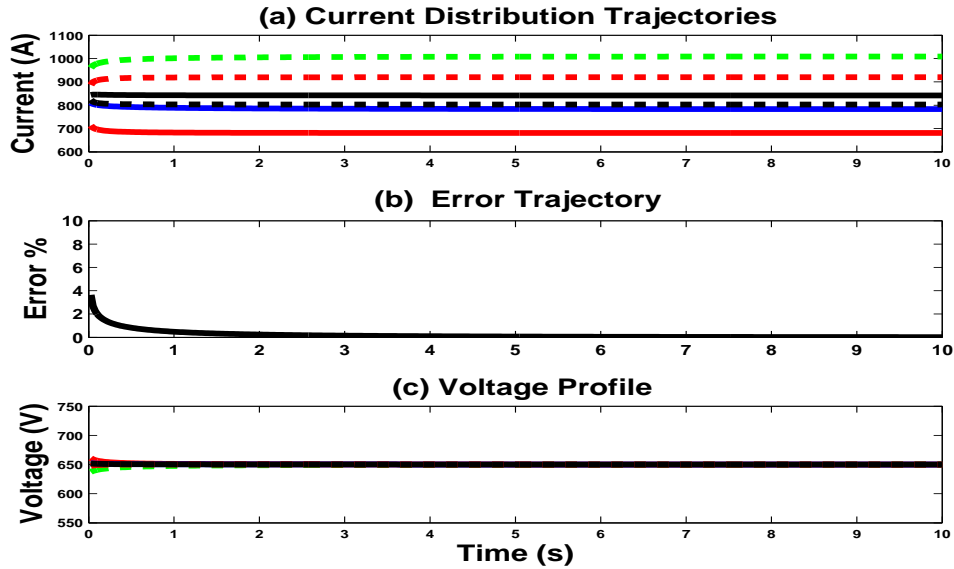Figure 5: Voltage trajectories under $a = 0.1$, $b = 0.3$ and $c = 0.6$

Figure 6: Voltage trajectories under $a = 0$, $b = 0$ and $c = 1$

Looking at the voltage profile, it is clearly seen that all node voltages are equal to the reference value, and the currents are equal to their corresponding local load $L(t) = [681, 783, 1009, 842, 921, 803]^T$.

3.5.4 Robustness to Load Disturbance

Trolleybuses systems experience very frequent and significant load disturbances due to vehicles' unpredictable power demands. As a result, the feeder currents will experience sudden changes so that the optimality is lost at the time of load disturbance. The control algorithm then uses local information exchange to correct such deviations and restore optimality at the new equilibrium point.

Suppose that there is a sudden increase in node 4's load at $t = 5$ (second) from 842 to 950 (A). Fig. 7 demonstrates the current trajectories of the feeders after the load disturbance using the weighting coefficients $a = 0.3$, $b = 0.2$ and $c = 0.5$, which converge asymptotically to the new optimal point of operation.
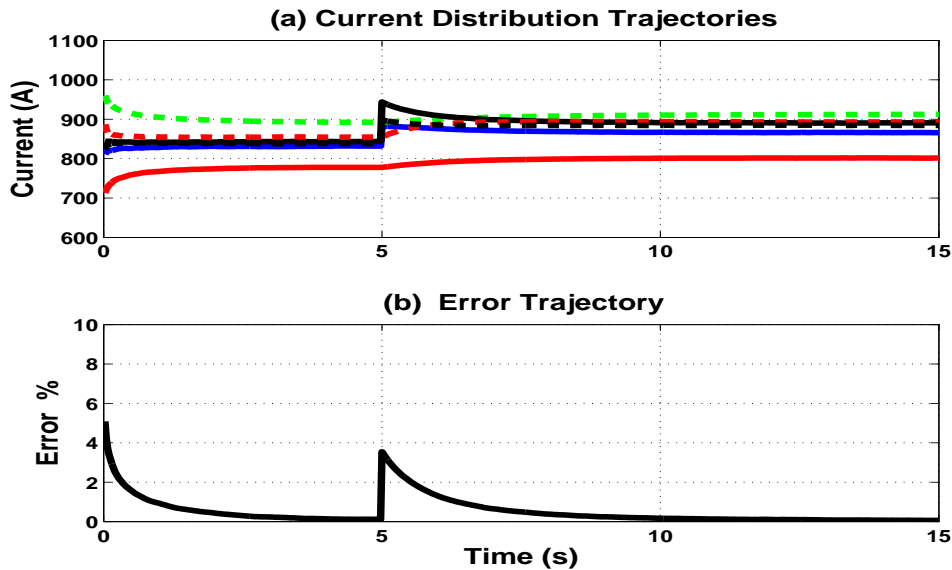

Figure 7: Robustness to load disturbance

To showcase the robustness even more, suppose there is a sudden increase in nodes' 2,4, and 6 from 811 (A) to 961 (A), 842 to 942 (A), and 823 to 883 (A) respectively. Fig.8 showcases the current trajectories and optimality error of such scenario using

the weighting coefficients $a = 0.3$, $b = 0.2$ and $c = 0.5$. It is clear that the trajectories converge asymptotically to the new optimal point of operation.
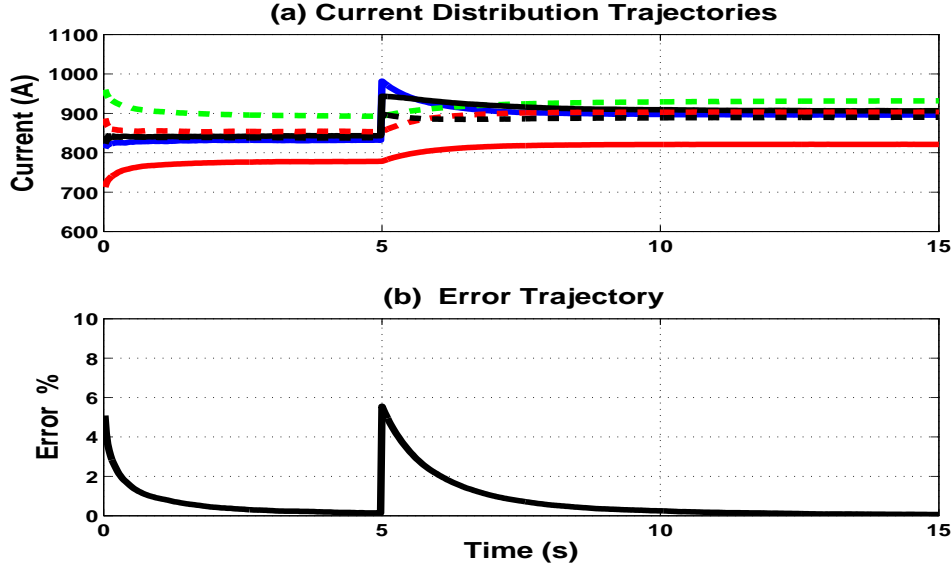

Figure 8: Robustness to a more extreme load disturbance

3.5.5   Scalability

Trolleybus systems are subject to structural changes. For example, a segment may be added after a maintenance service or a new construction, or removed due to power interruption. An appealing feature of distributed control is that adding or subtracting segments from the network only affects the neighboring segments. After removing a segment, the remaining segments must share the extra load. Similarly, when adding a new segment, it will have its share of the total load through distributed control.

First, suppose that a segment labeled as node 7 is added with its initial current $I_7 = (0)900$ (A) and load $L_7(0) = 920$ (A), connected to node 6 as shown in Fig. 9 with line resistance $R_{67} = 0.33$ (Ω).
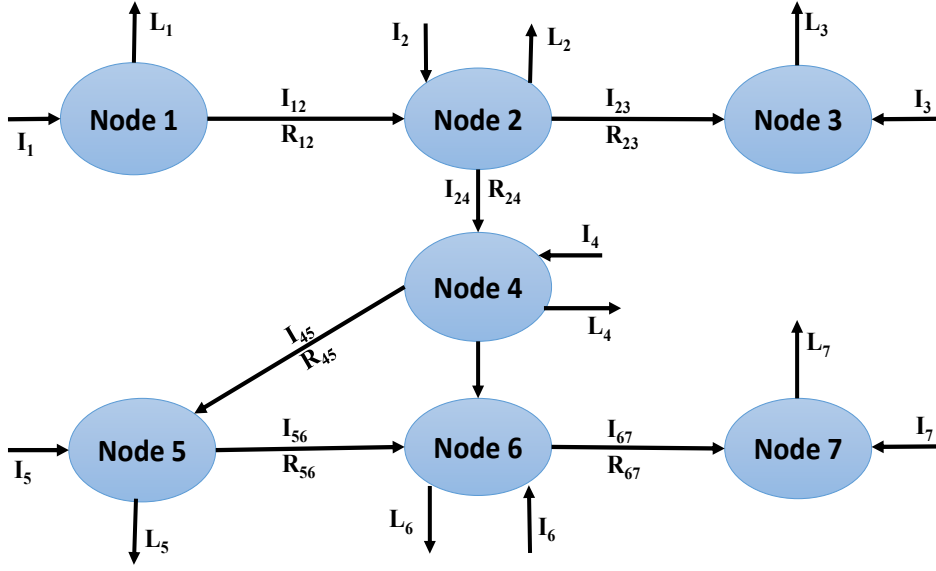
Figure 9: The expanded network topology after a node addition

Now, the trolleybus system has 7 feeders and 6 communication links $G = \{(1, 2),$ $(2, 3), (2, 4), (4, 5), (5, 6), (6, 7)\}$. The initial feeder currents are $I(0) = [713, 811, 981,$ $844, 887, 823, 900]^T$, the load vector is $L(t) = [681, 783, 1009, 842, 921, 803, 920]^T$, and the link currents are $y(t) = [I_{12}(t), I_{23}(t), I_{24}(t), I_{45}(t), I_{56}(t), I_{67}(t)]^T$. The line resistances are $R = \text{diag}[R_{12}, R_{23}, R_{24}, R_{45}, R_{56}, R_{67}] = \text{diag}[0.4, 0.38, 0.34, 0.31, 0.36, 0.33]$. The weighting coefficients remain as $a = 0.3$, $b = 0.2$ and $c = 0.5$.

After the new segment is added, the distributed control algorithm distributes the load fairly among all feeders in the modified power network. Fig. 10 shows the feeder currents converge to the optimal solution, evidenced by the convergence of optimality error trajectories to zero.

Similarly, the methodology can also be used when the network is reduced as shown in Fig. 11.
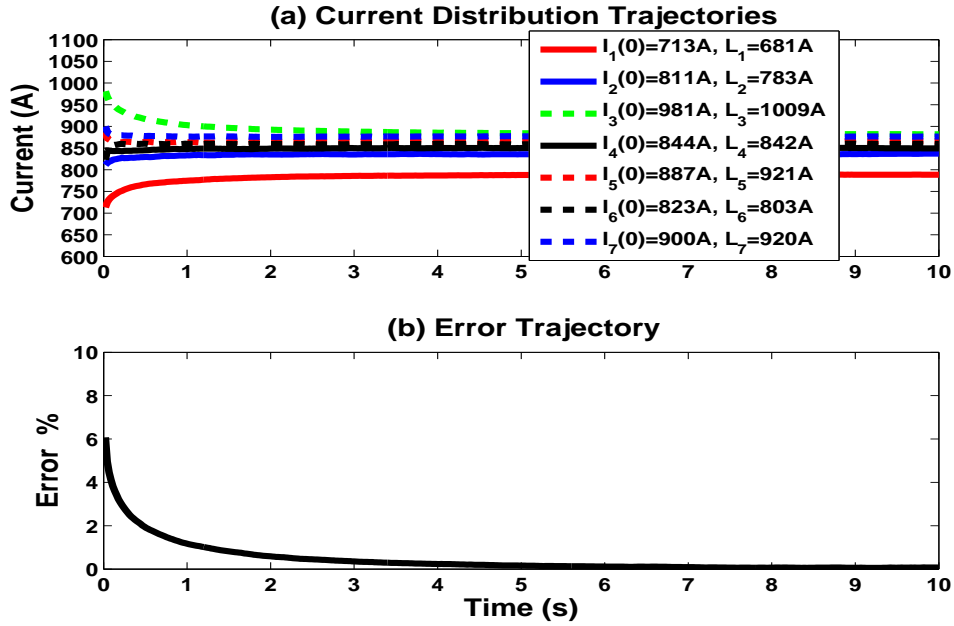
Figure 10: Feeder currents and error trajectories of the expanded system
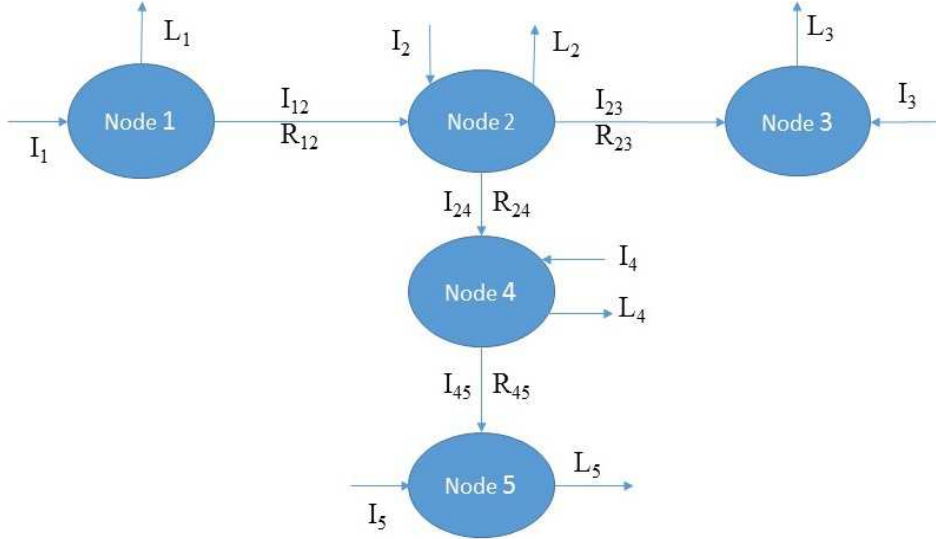
Figure 11: The 5-node network topology after one node is removed

The trolleybus system now has 5 feeders and 4 communication links $G = \{(1, 2),$ $(2, 3), (2, 4), (4, 5)\}$. The initial feeder currents are $I(0) = [713, 811, 960, 845, 907]^T$, the load vector is $L(t) = [681, 783, 1009, 842, 921]^T$, and the link currents are $y = [I_{12}(t), I_{23}(t), I_{24}(t), I_{45}(t)]^T$. The line resistances are $R = \text{diag}[R_{12}, R_{23}, R_{24}, R_{45}] =$

diag$[0.4, 0.38, 0.34, 0.31]$. The weighting coefficients are selected the same as previous cases $a = 0.3$, $b = 0.2$ and $c = 0.5$. Fig. 12 shows the feeder current trajectories and optimality error trajectories of the system when node 6 is removed from the system.
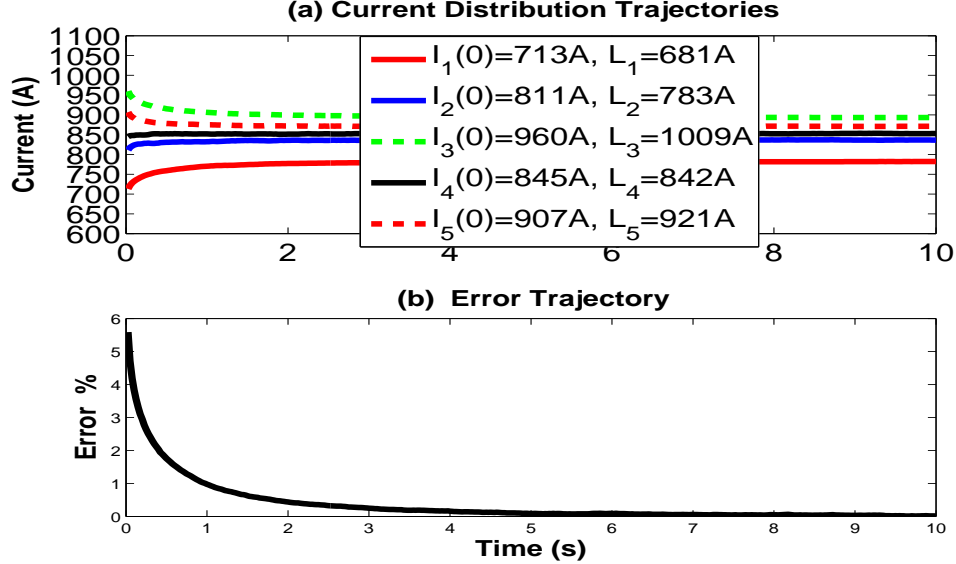
Figure 12: Feeder currents and error trajectories of the reduced system

3.5.6 Including Feeders with Different Capacities

We now apply our method to the case of different feeder capacities. Using the same weighting coefficients $a = 0.3$, $b = 0.2$ and $c = 0.5$ as before, this case study now considers feeders of different (relative) capacities with $\gamma_1 = 0.8, \gamma_2 = 0.9, \gamma_3 = 1.2, \gamma_4 = 1.05,$ $\gamma_5 = 1.1$ and $\gamma_6 = 0.95$. Note that the summation of the relative capacities of all feeders is equal to the number of nodes $r = 6$ $(\sum_{i=1}^{r} \gamma_i = r)$.[1] Thus, the nodes' relative capacity matrix Γ becomes $\Gamma = \mathrm{diag}[1/0.8, 1/0.9, 1/1.2, 1/1.05, 1/1.1, 1/0.95]$.

Fig.13 shows the currents trajectories and the optimality errors when using different feeders capacities. From subplot(a) of Fig. 13, it is clear that the higher the

---

[1] The previous uniform feeder capacities have $\gamma_1 = \cdots = \gamma_6 = 1$ whose summation is also 6.

relative capacity of the feeder is, the more that feeder supplies the network.
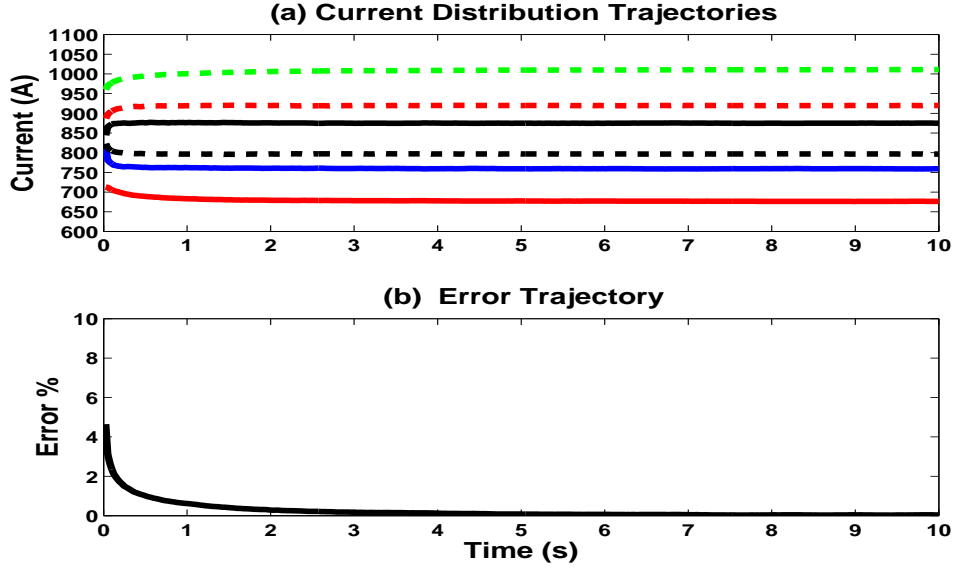
Figure 13: Feeder currents and error trajectories of the system with different capacities

3.5.7 Evaluation on a 14-bus DC System

In order to demonstrate that our methodology can be efficiently used in other DC microgrids, the method will be applied to a 14-bus DC system whose topology is shown in Fig 14.

Now, the system has 14 feeders and 13 communication links $G = \{(1,2), (2,3), (3,4), (3,5), (5,6), (6,7), (7,8), (8,9), (8,10), (8,11), (11,12), (12,13), (12,14)\}$. The initial feeder currents are $I(0) = [723, 810, 960, 845, 887, 825, 740, 790, 960, 844, 887, 823, 980, 680]^T$, the load vector is $L(t) = [850, 783, 1009, 802, 960, 800, 640, 740, 1009, 690, 921, 800, 950, 800]^T$, the line resistances are $R = \text{diag}[R_{12}, R_{23}, R_{44}, R_{35}, R_{56}, R_{67}, R_{78}, R_{89}, R_{8-10}, R_{8-11}, R_{11-12}, R_{12-13}, R_{12-14}] = \text{diag}[0.4, 0.38, 0.34, 0.31, 0.36, 0.35, 0.4, 0.42, 0.37, 0.34, 0.36, 0.4, 0.39]$. The weighting coefficients are selected as $a = 0.3$,
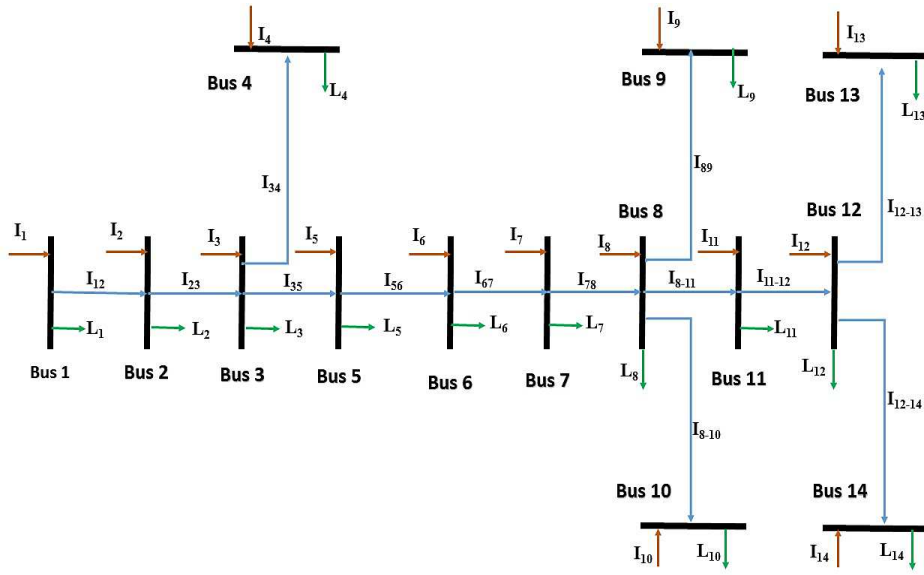
Figure 14: The 14-bus DC system network topology

$b = 0.2$ and $c = 0.5$.

Fig. 15 shows the simulation results. Subplot (a) shows that the feeders' currents converge to their final values. Subplot (b) demonstrates global optimality of our algorithm by showing that the errors between the performance values achieved by the distributed recursive algorithm and the global optimum.
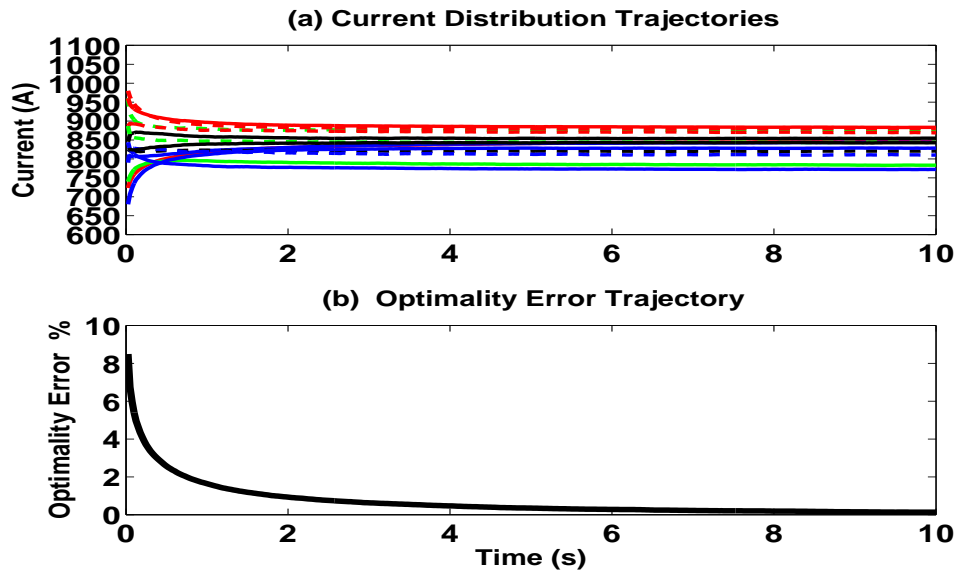
Figure 15: Feeder currents and error trajectories of the 14-bus DC System

For extended methodology evaluation on the 14- Bus DC System, Fig.16 shows the feeder's current trajectories and optimality error when there is a disturbance happening in the load side. An increase of 50 (A), 100 (A), 90 (A) and 150 (A) occurs to the loads of nodes 2, 4, 6 and 9 respectively.
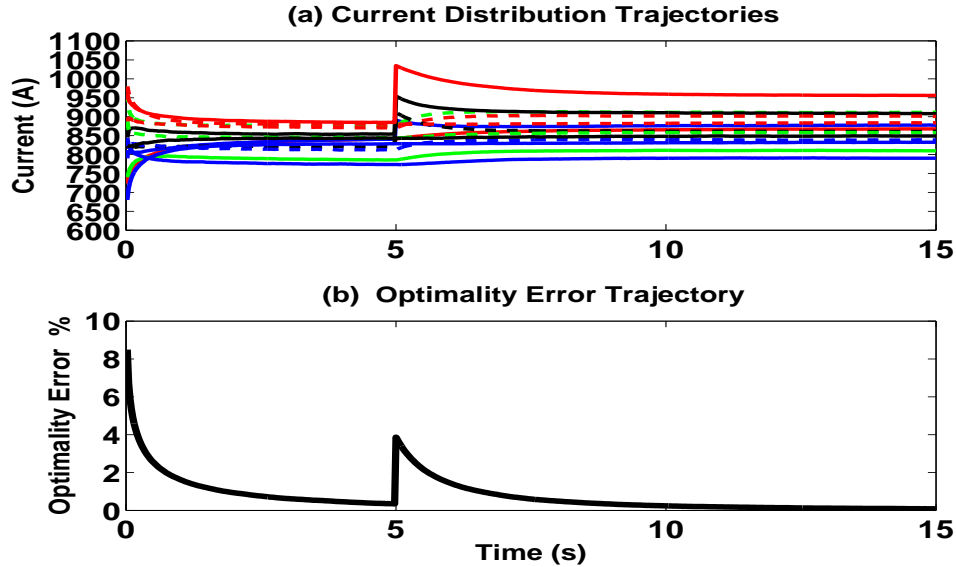
Figure 16: The 14-bus DC system network topology with load disturbance

Fig.16 demonstrates that the current trajectories converge asymptotically to the new optimal point of operation.

3.5.8 Guidelines on Selecting Weights

Selection of the weights a, b, and c is a practical matter and highly problem specific. They provide a tuning mechanism to define the optimization problem to accommodate specific needs.

Due to system coupling, the three control objectives cannot be achieved simultaneously. In principle, if load assignment to feeders is more critical, a needs to be

increased. This is exemplified by the scenarios of heavily loaded feeders and the desire to fully utilize the existing MG to support more loads. On the other hand, if voltage excursions under certain contingent conditions are too large, c needs to be increased. Similarly, when feeder capacities are sufficient and voltage profiles are well within their limits, a and c could be reduced, but b is increased so that power loss can be reduced. Such a calibration process is inherent in all multi-objective optimization problems and is considered one critical step in control design.

To elaborate more on what has been said, Fig. 17 shows a set of consensus error curves in which the weighting coefficient a is changed from $1, 0.8, 0.6, 0.4, 0.2$ with b and c share the remaining value.
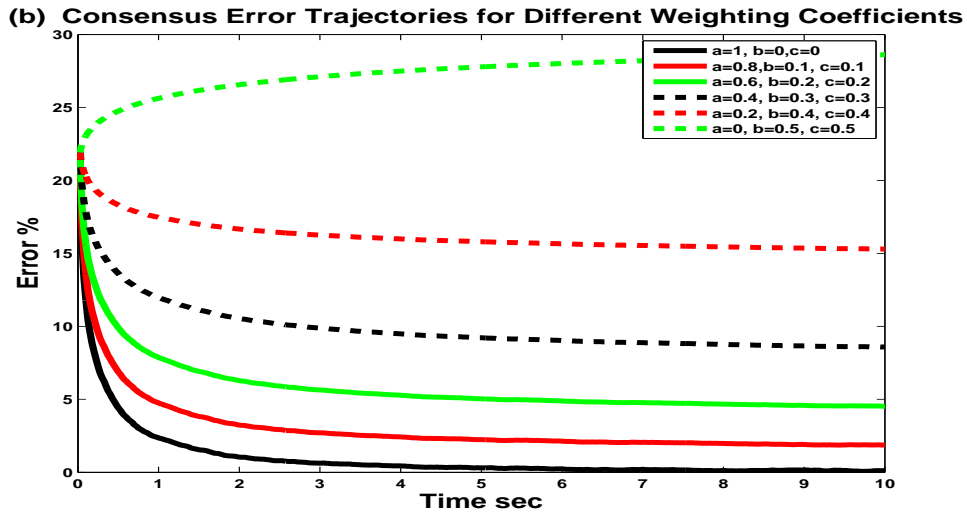
Figure 17: Consensus error using gradual change in the weighting coefficient a

Similarly, Fig. 18 shows a set of voltage errors from the reference voltage in which the weighting coefficient c is changed from $1, 0.8, 0.6, 0.4, 0.2$ with a and b share the remaining value.
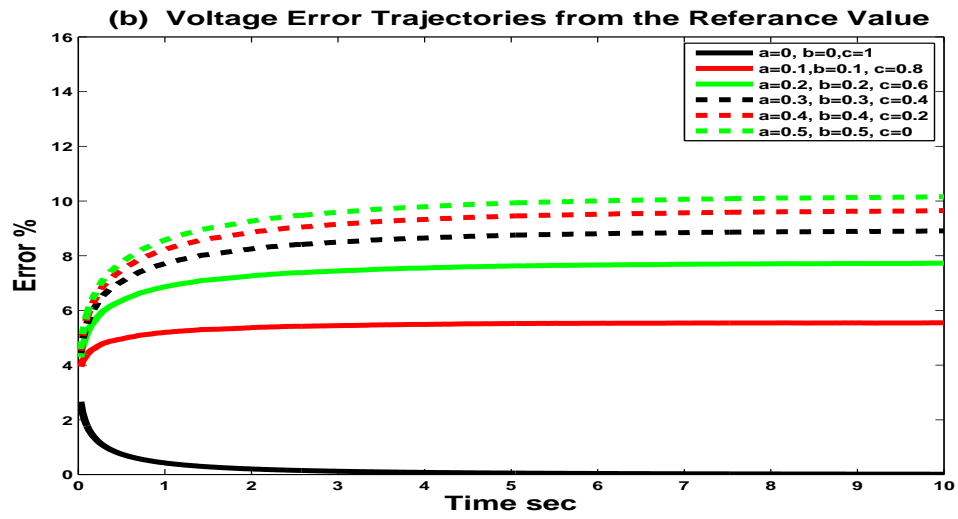
Figure 18: Voltage error from the reference value using gradual change in the weighting coefficient c

4 INCLUSION OF SUBSYSTEM DYNAMICS

This chapter introduces a distributed methodology based on the one in the previous chapter that includes subsystem dynamics. The chapter is organized into the following sections. Section4.1 gives a quick literature review on proposed work in this chapter. Section 4.2 formulates the main problems. The algorithms are introduced in Section 4.4. The main properties of the algorithms are established. Finally, section 4.5 presents case studies to demonstrate the performance of the proposed algorithms.

4 Introduction

Continuing on the distributed optimization strategies introduced in the previous chapter for optimal load sharing, loss reduction and voltage quality in optimization in DC microgrids, the framework is further extended to include subsystem dynamics. Inclusion of subsystem dynamics accommodates many real systems, especially converter dynamics, impacts performance significantly, and complicates system analysis are introduced in this part of the work.

For distribution power systems with renewable and distributed generators, see [1, 2]. Centralized, decentralized, distributed control methods for power grid management have been extensively studied in the recent years [3, 4, 5, 6, 7]. For different performance considerations, power losses have been considered in many MGs [13, 14, 15, 9]. Within centralized strategies, global optimality has been analyzed in [16]. On the other hand, the traditional frequency and voltage droop control methods for standing-alone MGs are decentralized [17, 19, 20, 21]. Distributed strategies have been pursued in recent years [24, 25] with some promising new methodologies [19, 26]. A consensus method was introduced to power system load distribution in [31]. These results do not include distributed optimization with subsystem dynamics.

The control methodology of this part retains the key advantages: (1) It requires only neighborhood information exchange among nodes in the network. (2) The local optimization can achieve the global optimization. This is especially important for a large network with physically distributed subsystems. (3) It has provable properties

of convergence to the global minima under noisy observations. (4) It is robust against load perturbations and allows reconfiguration with subsystem addition and deletion. (5) It is scalable in the sense that system expansion will not significantly increase control system complexity. By accommodating subsystem dynamics, the new algorithms have broader applications and more realistic conditions.

4 Problem Formulation

The problem formulation of this chapter follows what was presented in Chapter (3). The main difference is that the subsystem dynamics are now included. Since subsystems' physical dynamics have an essential impact of stability and convergence, the methodology in this chapter is different from what has been introduced in the previous chapter.

4.2.1 Equality Constraints

The same DC networks used in the first part is also used here to illustrate the main variables and concepts, and is included in here; see Fig. 19, for illustration and case studies.

Figure 19: A DC microgrid with 6 feeders and 5 links.
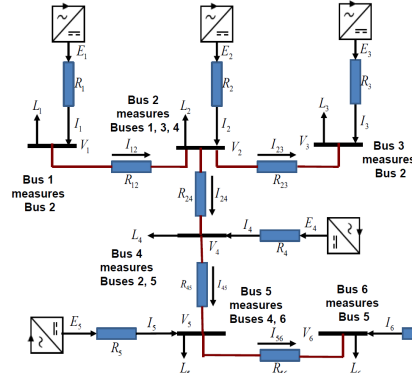
For this DC power network, the real-time supply current of the ith node is $I_i(t)$ (A), its load is $L_i(t)$ (A), and the node voltage is $v_i(t)$ (V) noting that the word "node" represents a feeder line, a bus, etc. The network topology is represented by a directed graph G. For $(i, j) \in G$, the current from the ith node to the jth node is $I_{ij}(t)$ (A),

and the line resistance is R_{ij} (Ω), and $I_{ij} = -I_{ji}$. Denote $u(t) = [I_1(t), \ldots, I_r(t)]^T$, $v(t) = [v_1(t), \ldots, v_r(t)]^T$, $L(t) = [L_1(t), \ldots, L_r(t)]^T$. By specifying a given order of the links, y is the column vector of the link currents, $R = \text{diag}[R_{ij}]$ is the link resistance matrix. The supply line of the ith node has rated current capacity γ_i. Define $\Gamma = \text{diag}[1/\gamma_i]$ and $\gamma = [\gamma_1, \ldots, \gamma_r]^T$. For the 6-node DC MG in Fig. 19, $G = \{(1,2), (2,3), (2,4), (4,5), (5,6)\}$ and $l_s = 5$, $y = [I_{12}(t), I_{23}(t), I_{24}(t), I_{45}(t), I_{56}(t)]^T$, $R = \text{diag}[R_{12}, R_{23}, R_{24}, R_{45}, R_{56}]$.

Assumption 3 (1) The DC MG is connected, but no loops. (2) The node communicates only with its physically connected neighbors. (3) Each node knows its own state and parameters. (4) Each node knows the link current and link resistance that is connected to it. (5) Each node knows its neighbor's rated capacity, but must estimate its neighbor's supply current with possible errors.

The following relationships are elementary from the basic circuit laws:

$$u = My + L \tag{4.1}$$

where M is an $r \times (r-1)$ network matrix, satisfying $M^T \mathbb{1} = 0$, where $\mathbb{1}$ is the column vector of all 1's and M is full column rank, and hence

$$y = (M^T M)^{-1} M^T (u - L). \tag{4.2}$$

The voltage law implies

$$M^T v = R y. \tag{4.3}$$

Following the tradition of power systems, an extra condition is given by

$$\zeta_o v = v_{ref}, \text{ with } \zeta_o \mathbb{1} = 1. \tag{4.4}$$

For example, if node 1 is designated as a reference bus whose voltage is independently controlled to be v_{ref}, then $\zeta_o = [1, 0, \ldots, 0]$.

By adding (4.4) to (4.3), we have $H_0 v = R_0 y + W v_{ref}$, where

$$H_0 = \begin{bmatrix} M^T \\ \zeta_o \end{bmatrix}, R_0 = \begin{bmatrix} R \\ 0, \ldots, 0 \end{bmatrix}, W = \begin{bmatrix} [0, \ldots, 0]^T \\ 1 \end{bmatrix}.$$

Since M depends only on the network topology and C is pre-determined, H_0 depends only on the system structure but not system parameters.

When the DC MG is connected, H_0 is full rank, $v = H_0^{-1} R_0 y + H_0^{-1} W v_{ref}$, and $H_0 \mathbb{1} = \begin{bmatrix} 0, \ldots, 0, 1 \end{bmatrix}^T = W$, which implies that $H_0^{-1} W = \mathbb{1}$. Furthermore, $H_0^{-1} R_0$ can be expressed as

$$H_0^{-1} R_0 = H_0^{-1} \begin{bmatrix} R \\ 0 \end{bmatrix} = H_0^{-1} \begin{bmatrix} I \\ 0 \end{bmatrix} R = QR$$

in which $Q = H_0^{-1} \begin{bmatrix} I \\ 0 \end{bmatrix}$ depends only on the network topology, but not on the network parameters R_{ij}. Leading to

$$v = QRy + v_{ref}\mathbb{1}. \tag{4.5}$$

It can be verified that Q has rank $r - 1$, and hence $Q^T Q$ is full rank.

4.2.2 Performance Index and Distributed Optimization

Without consideration of subsystem dynamics, a multi-objective performance index was introduced in section 3.2. Define a weighting matrix $\Phi = Q(Q^T Q)^{-1}(Q^T Q)^{-1}Q^T$, and

$$J = \frac{1}{2}[a(u - \beta\gamma)^T \Gamma(u - \beta\gamma) + by^T Ry + c(v - v_{ref}\mathbb{1})^T \Phi(v - v_{ref}\mathbb{1})] \tag{4.6}$$

subject to the constraints (4.1) and (4.5). This performance index represents a tradeoff among the load distribution to suppliers (the first term), the power loss on the transmission line (the second term), and voltage quality (the third term). The weights $a, b, c \geq 0$ with $a + b + c = 1$ are used to tune a desired trade-off among the three objectives.

Denote $\Gamma^{1/2} = \text{diag}[1/\sqrt{\gamma_i}]$, $M_0 = \Gamma^{1/2}M$, and $L_0 = \Gamma^{1/2}L$. Under the relations (4.1) and (4.5), the performance index (4.6) becomes

$$J(y) = \tfrac{1}{2}[a(M_0 y + L_0 - \beta\Gamma^{1/2}\gamma)^T(M_0 y + L_0 - \beta\Gamma^{1/2}\gamma)$$

$$+ by^T Ry + cy^T R^2 y].$$

Consequently, the link current vector y becomes naturally the control variable. Our objective is to minimize the performance index

$$\min_{y} J(y). \tag{4.7}$$

The following results are from section 3.2 and section 3.3 respectively.

Theorem 4 *The global optimal solution to* (4.7) *is*

$$y^* = -[aM_0^T M_0 + bR + cR^2]^{-1} aM_0^T L_0. \tag{4.8}$$

Proof: In order to solve the optimization problem, we calculate the stationary point

$$\frac{\partial J(y)}{\partial y} = aM_0^T(M_0 y + L_0 - \beta\Gamma^{1/2}\gamma) + bRy + cR^2 y$$

$$= [aM_0^T M_0 + bR + cR^2]y + aM_0^T L_0 - aM_0^T \beta\Gamma^{1/2}\gamma$$

$$= 0.$$

Where,

$$M_0^T \Gamma^{1/2}\gamma = M^T\Gamma\gamma = M^T\mathbb{1} = 0$$

is used in the derivation. The optimal link current vector y^* is

$$y^* = -[aM_0^T M_0 + bR + cR^2]^{-1} aM_0^T L_0.$$

Also, the Hessian matrix is

$$a M_0^T M_0 + bR + cR^2.$$

This matrix is positive definite because $M_0^T M_0 > 0$, $R > 0$, $R^2 > 0$ as long as one of the coefficients is positive. Which implies that y^* is indeed the minimum point. $\square$

For each link $(i, j) \in G$, the local objective function is defined as

$$J_{ij} = \frac{1}{2} [\frac{a}{2} \left(\frac{I_i}{\gamma_i} - \frac{I_j}{\gamma_j} \right)^2 + bR_{ij} I_{ij}^2 + cR_{ij}^2 I_{ij}^2]. \tag{4.9}$$

Theorem 5 *The local optimal solutions to* (4.9) *are identical to the global optimal solution* (4.8).

Proof: The optimal link current I_{ij} can be derived locally from the local optimality condition

$$\begin{aligned}
\frac{\partial J_{ij}}{\partial I_{ij}} &= \frac{a}{2} \left(\frac{I_i}{\gamma_i} - \frac{I_j}{\gamma_j} \right) \left(\frac{\partial I_i}{\partial I_{ij}} - \frac{\partial I_j}{\partial I_{ij}} \right) + bR_{ij} I_{ij} + cR_{ij}^2 I_{ij} \\
&= a \left(\frac{I_i}{\gamma_i} - \frac{I_j}{\gamma_j} \right) + bR_{ij} I_{ij} + cR_{ij}^2 I_{ij} \\
&= 0,
\end{aligned}$$

where the facts $\frac{\partial I_i}{\partial I_{ij}} = 1$ and $\frac{\partial I_j}{\partial I_{ij}} = -1$ have been applied.

Since

$$\frac{\partial^2 J_{ij}}{\partial I_{ij}^2} = a \left(\frac{1}{\gamma_i} + \frac{1}{\gamma_j} \right) + bR_{ij} + cR_{ij}^2 > 0,$$

Then, this is indeed the local minimum point.

By considering all the links and expressing them in matrix form, the local optimality condition becomes

$$aM^T\Gamma u + bRy + cR^2 y = 0. \tag{4.10}$$

By using (4.1), $M^T\Gamma M = M_0^T M_0$, and $M^T\Gamma L = M_0^T L_0$, we have

$$aM^T\Gamma(My + L) + bRy + cR^2 y = 0,$$

or

$$[aM_0^T M_0 + bR + cR^2]y + aM_0^T L_0 = 0,$$

which is identical to (4.8) $\qquad\qquad\square$

The original distributed control updating algorithm, without consideration of subsystem dynamics, is given in section 3.4 eqn. (3.13) as

$$u_{n+1} = u_n - \mu_n M\Pi[aM^T\Gamma u_n + bRy_n + cR^2 y_n - ad_n], \tag{4.11}$$

where $\{d_n\}$ is a sequence of observation noise vectors, $\{\mu_n\}$ is a sequence of step sizes satisfying appropriate conditions; $\Pi = \text{diag}[g_{ij}]$ is the $(r-1) \times (r-1)$ diagonal matrix of the same order as R, $g_{ij} > 0$ is the link specific gain to allow different feedback gains on different links.

4 Subsystem Dynamics and System Integration

4.3.1 General Structure of Local Dynamics and Control Design

When the subsystem dynamics are included, the desired feeder currents calculated by the distributed optimization algorithm cannot be implemented immediately. Instead, local power converter control systems will try to control the feeder currents to follow the desired values which will be served as the reference input and command signals, which will be denoted by z_j, to distinguish them from the actual feeder currents $u_j = I_j$, $j = 1, \ldots, r$.

For the jth subsystem, its power converter's control signal is the duty cycle $\delta_o j$ and the output is the actual feeder current $u_j = I_j$. The power converter dynamics can be represented by a linearized system P_j. The converter controller F_j acts on the difference $e_j = z_j - u_j$, leading to $\delta_o j = F_j e_j$. Together, the closed-loop system from z_j to u_j is

$$M_j = \frac{F_j P_j}{1 + F_j P_j}. \tag{4.12}$$

For algorithm development, it is assumed that M_j can be realized by a state space model

$$\dot{x}_j = A_j x_j + B_j z_j; u_j = C_j x_j, j = 1, \ldots, r. \tag{4.13}$$

We emphasize that (4.13) is the model for the closed loop systems.

Assumption 4 (1) The closed-loop system (4.13) is asymptotically stable. (2) The steady-state tracking error is zero. Namely, $\lim_{t \to \infty} (z_j(t) - u_j(t)) = 0$.

By combining these subsystem dynamics for the entire network, we have

$$\dot{x} = Ax + Bz, u = Cx, \tag{4.14}$$

where $x = [x_1, \ldots, x_r]'$, $u = [u_1, \ldots, u_r]'$, $z = [z_1, \ldots, z_r]'$, $A = \mathrm{diag}[A_j]$, $B = \mathrm{diag}[B_j]$, $C = \mathrm{diag}[C_j]$. It is noted that local controller design will affect the closed-loop system M_j, and hence it will affect overall algorithm stability and performance. This will be discussed in our case studies.

4.3.2 System Integration

By selecting a small and possibly time-varying sampling interval $\tau_n > 0$, the system can be sampled, resulting in a discrete-time system

$$x_{n+1} = x_n + \tau_n(Ax_n + Bz_n), u_n = Cx_n. \tag{4.15}$$

The coordination algorithm (4.11) must be modified by using the actual feeder current information u_n in its updating of the desired values z_n. It follows that the new coordination algorithm takes the form of

$$
\begin{aligned}
z_{n+1} &= z_n - \mu_n M\Pi[aM^T\Gamma u_n + bRy_n + cR^2y_n - ad_n] \\
u_{n+1} &= u_n + \tau_n C(Ax_n + Bz_n)
\end{aligned}
\tag{4.16}
$$

and $y_n = (M^T M)^{-1}M^T(u_n - L_n)$. The interaction between the coordination algorithm and the local dynamics is realized by u_n and y_n in the former, and z_n in the latter.

The interaction is significantly affected by the choice of μ_n and τ_n. We will show that by choosing $\tau_n = \alpha\mu_n$, the stability of the integrated system can be rigorously established. Let $\tau_n = \alpha\mu_n$, where $\alpha > 0$ is to be designed. This results in

$$
\begin{aligned}
z_{n+1} &= z_n - \mu_n M\Pi[aM^T\Gamma u_n + bRy_n + cR^2 y_n - ad_n] \\
u_{n+1} &= u_n + \mu_n \alpha C(Ax_n + Bz_n)
\end{aligned}
\tag{4.17}
$$

4 Convergence Analysis

This section analyzes the proposed algorithm. The convergence is established using the ODE methods in a similar fashion to the convergence analysis in section 3.4.

Assumption 5 *(1) The noise $\{d_n\}$ is a stationary ϕ-mixing sequence such that $Ed_n = 0$, $Ed_n^{2+\Delta} < \infty$ for some $\Delta > 0$, and that the mixing measure $\tilde{\phi}_n$ satisfies $\sum_{k=0}^{\infty} \tilde{\phi}_k^{\frac{\Delta}{(1+\Delta)}} < \infty$, where E is the expectation, and P is the probability. (2) $\{\mu_n\}$ is a sequence of step sizes satisfying $\mu_n \geq 0$, $\mu_n \to 0$ as $n \to \infty$, and $\sum_{k=0}^{\infty} \mu_k = \infty$.*

The ϕ-mixing sequence is more realistic and allows the observation noises to be correlated. Algorithm (4.17) is a stochastic approximation algorithm, whose convergence properties can be established by using the ODE method.

To summarize the steps in proving convergence properties, we define $t_n = \sum_{k=0}^{n-1} \mu_k$. Let $u^0(t)$ and $z^0(t)$ be a piecewise constant interpolation of u_n and z_n on the interval $[t_n, t_{n+1})$, respectively, and $u^n(t) = u^0(t + t_n)$ and $z^n(t) = z^0(t + t_n)$ be their shifted sequences. Denote $m(t) = \max\{n : t_n \leq t\}$. By the relationship $y = (M^T M)^{-1} M^T (u - L)$, also $y^n(t) = (M^T M)^{-1} M^T \Gamma(u^n(t) - L)$. The sequence $\{u^n(\cdot)\}$ (and $\{z^n(\cdot)\}$, $\{y^n(\cdot)\}$) is in an appropriate function space that is uniformly bounded and equi-continuous in the extended sense. By using the extended version of the Arzela-Ascoli Theorem (see [59]), it can be shown that $\{u^n(\cdot)\}$ (and $\{z^n(\cdot)\}$, $\{y^n(\cdot)\}$) has a convergent subsequence with limit $u(\cdot)$ (and $y(\cdot)$, $z(\cdot)$) such that $u(\cdot)$

satisfies the ordinary differential equation

$$\dot{z} = -M\Pi[aM^T\Gamma u + bRy + cR^2 y]$$

$$\dot{x} = \alpha(Ax + Bz) \tag{4.18}$$

$$u = Cx, \ \ y = (M^T M)^{-1} M^T (u - L)$$

It can be derived that for sufficiently small α the equilibrium point of the ODE is the solution to to the global optimal solution. The stability of the limit ODE can also be established. The proof of the next Theorem is omitted since it is similar to that of Theorem 3 in section 3.4.

Theorem 6 *Under Assumption 3, $y^n(\cdot + q_n) \to y^*$ with probability 1 as $n \to \infty$, where $q_n \to \infty$ as $n \to \infty$ and y^* is the stable stationary point of the ODE (4.18).*

4 Case Studies

Consider the trolleybus system in Fig. 19. The system has six nodes (segments), and five communication links represented by $G = \{(1,2), (2,3), (2,4), (4,5), (5,6)\}$. The feeders' initial currents are $I(0) = [713, 811, 960, 844, 887, 823]^T$ (A) while the local loads are $L(t) = [681, 783, 1009, 842, 921, 803]^T$.

The link currents are labeled as $y(t) = [I_{12}(t), I_{23}(t), I_{24}(t), I_{45}(t), I_{56}(t)]^T$. The line resistances are calculated based on the station supply radii with values $R = \text{diag}[R_{12}, R_{23}, R_{24}, R_{45}, R_{56}] = \text{diag}[0.4, 0.38, 0.34, 0.31, 0.36]$ (Ω). The rated bus voltage is 650 (V). Typically, in the trolleybus systems the voltage variations are allowed for 10%, namely in the range of $[585, 715]$.

4.5.1 Power Converter Dynamics and Local Controller

For the trolley bus system with 6 nodes, there are six Buck DC-DC converters. The topology used for those converters is shown in Fig. 20:
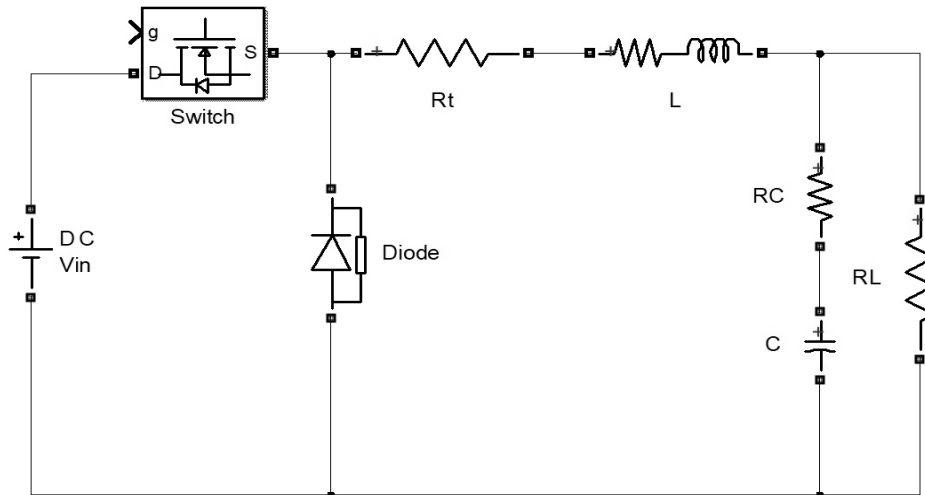

Figure 20: DC-DC Buck converter topology

Where: R is the inductance resistance, R_L is the load resistance, R_t is the sensing resistance, R_c is the capacitances resistance, L is the inductance and C is the capacitance.

Impedance modeling is used to derive the transfer function $P(s) = \frac{I_o(s)}{D(s)}$ of the converter from the duty cycle δ_o $(D(s))$ to the output current I_o as follows.

$$Z_c(s) = R_c + \frac{1}{cs}$$

$$Z_L(s) = R_l + Ls$$

$$Z_1 = Z_c//R_L = \frac{R_L Z_c}{R_L + Z_c}$$

$$Z = Z_1 + Z_L + R_t$$

$$\frac{V_o(s)}{D(s)} = V_{in} P_1(s) Z_1(s)$$

$$P_1(s) = \frac{1}{Z(s)}$$

$$I_o(s) = \frac{V_o(s)}{R_L},$$

$$P(s) = \frac{I_o(s)}{D(s)} = \frac{V_{in} P_1(s) Z_1(s)}{R_L}.$$

For the ith feeder, its plant model $P_i(s)$ can be realized in a state-space model

$$\dot{x}_p^i(t) = A_p^i x_p^i(t) + B_p^i \delta_i(t), \quad I_o^i(t) = C_p^i x_p^i(t),$$

or collectively, with obvious vector variables and diagonal matrix expressions,

$$\dot{x}_p = A_p x_p + B_p \delta, \quad u = C_p x_p.$$

Here $u = [I_o^1, \ldots, I_o^6]^T$ is the actual feeder currents.

A power-electronic local controller F_i is designed so that the actual feeder current $u_i(t)$ can follow the desired $z_i(t)$: Let $e_i = z_i - u_i$. Then $\delta_o i = F_i e_i$. Typical converter controllers are PI controllers, $F_i(s) = K_p^i + \frac{K_I^i}{s}$, which can be written in a state space model

$$\dot{x}_F^i = e_i, \quad \delta_o i = K_I^i x_F^i + K_p^i e_i.$$

Collectively, the local controllers can be written as

$$\dot{x}_F = e, \quad \delta_o = K_I x_F + K_p e$$

in which the obvious compatible vectors and matrices are used.

The closed-loop subsystems can be derived, with the desired feeder currents z as the input and the actual feeder currents u as the output, as follows.

$$\dot{x}_p = A_p x_p + B_p \delta_o$$
$$= A_p x_p + B_p K_I x_F + B_p K_p e$$
$$= A_p x_p + B_p K_I x_F + B_p K_p z - B_p K_p u$$
$$= (A_p - B_p K_p C_p) x_p + B_p K_I x_F + B_p K_p z,$$
$$\dot{x}_F = e$$
$$= z - u$$
$$= -C_p x_p + z.$$

The output equation is $u = C_p x_p$. These lead to the final state space model (4.13)

for the closed-loop subsystems. We now use several simulation scenarios to illustrate our algorithms and performance.

4.5.2 Comparison to Trolleybus System Without Including the Dynamics

In order to convey the effect of including the converters' dynamics, it is needed to showcase the behavior of the system without those dynamics. Fig. 21 is reproduced from the previous chapter, which shows the system's behavior for such a case.
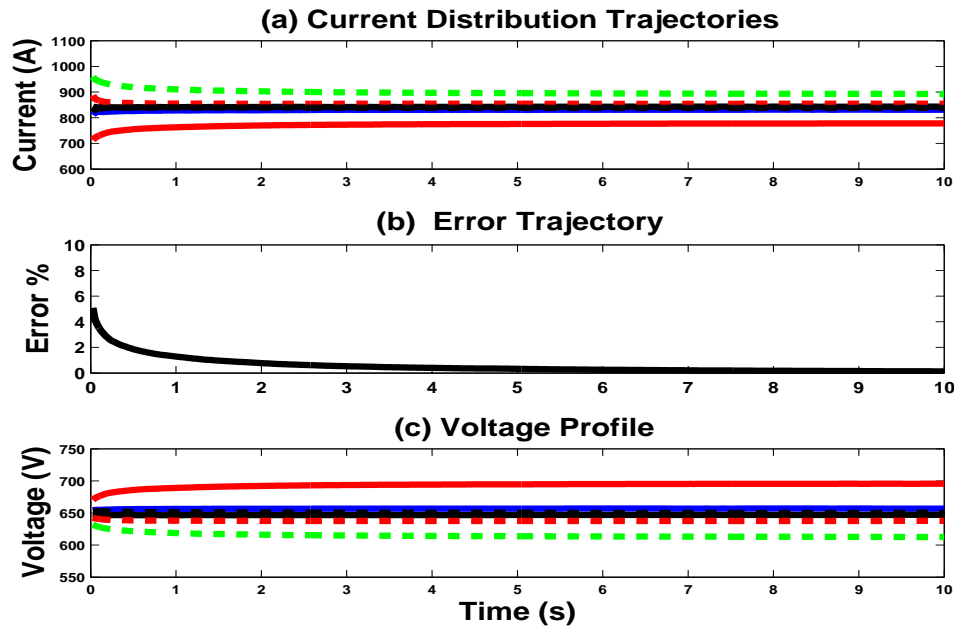
Figure 21: Feeder currents, optimality error trajectory, and voltage profiles under $a = 0.3$, $b = 0.2$ and $c = 0.5$

Subplot (a) shows that the feeders' currents converge to their final values. Subplot (b) is the error trajectory of the differences between the performance levels that are achieved by the distributed recursive algorithm and the global optimum. Subplot (c) shows the voltage profile. Due to the system dynamics, the execution of control actions is going to face performance limitations such as steady-state errors, overshoot

and settling time.

When introducing those dynamics, the converter signal processing sampling period is introduced. The actual convergence speed of feeders' current control is determined by how fast the converters can be controlled to follow the desired feeder current of each converter. Table 2 shows the values of the converters' parameters that will be used in the case studies.

	R_t	R	L	C	R_c	R_L
	Ω	Ω	mH	mF	Ω	Ω
Q_1	0.1	0.01	22.5	232	0.09	0.893
Q_2	0.1	0.01	22.5	232	0.09	0.79
Q_3	0.1	0.01	22.5	232	0.09	0.687
Q_4	0.1	0.01	22.5	232	0.09	0.767
Q_5	0.1	0.01	22.5	232	0.09	0.746
Q_6	0.1	0.01	22.5	232	0.09	0.776

Table 2: Circuit elements for each converter

Using the same example from the original case study, Fig.22 shows the system's behavior when the dynamics of the converters' are present.
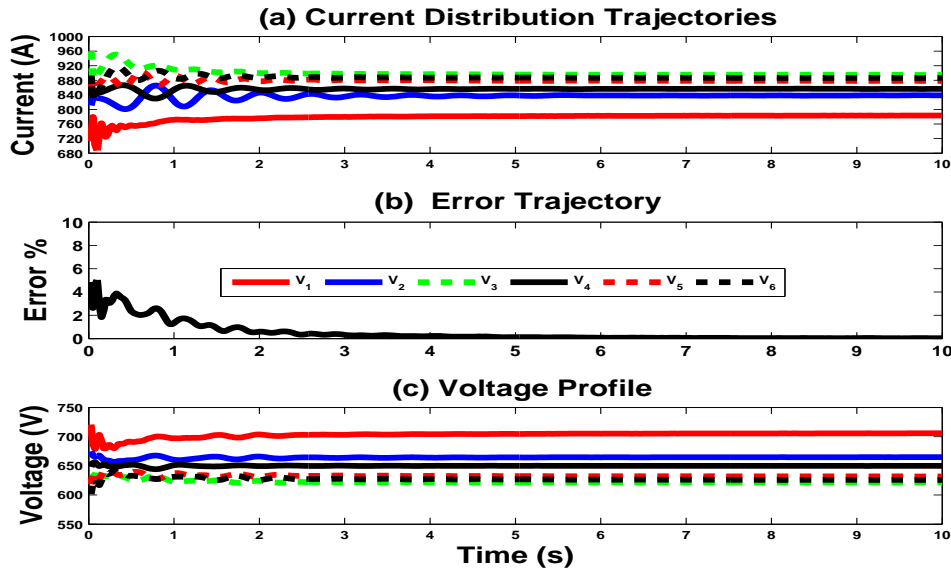

Figure 22: Feeder currents, optimality error trajectory, and voltage profiles in the presence of dynamics

The difference between the system's behavior when the dynamics are present is clearly seen. There is a noticeable overshoot/undershoot and oscillation compared to the original case study.

4.5.3 Impact of Converter PI Control

Suppose that a more aggressive controller compared to the previous example is used to force a faster settling time for each of the corresponding converter's response. The goal would be to force a faster convergence rate. Choosing suitable gains for the proportional and integral parts of the controller is important.

First, controller 2 was selected to showcase a faster response for Feeder 2 and the system as a whole. Fig. 23 shows the response of the system when such measures are taken.
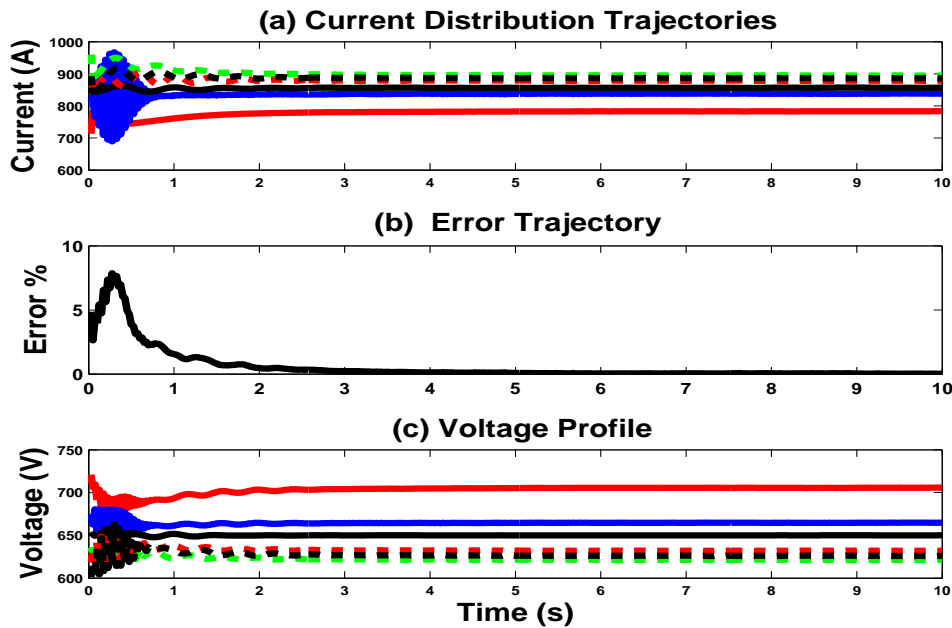
Figure 23: Feeder currents, optimality error trajectory, and voltage profiles when controller's 2 gains are selected as $K_P = 0.02018$ and $K_I = 0.02018$

Noticeable oscillations are occurring when controller's 2 gains are selected as $K_P = 0.02018$ and $K_I = 0.02018$. On the other hand, using a balanced tuning method in the selection of the proportional and integral gains of each converter's controller will bear better results compared to the original case study. Fig.24 shows the behavior of the system after tuning the controllers of each converter.

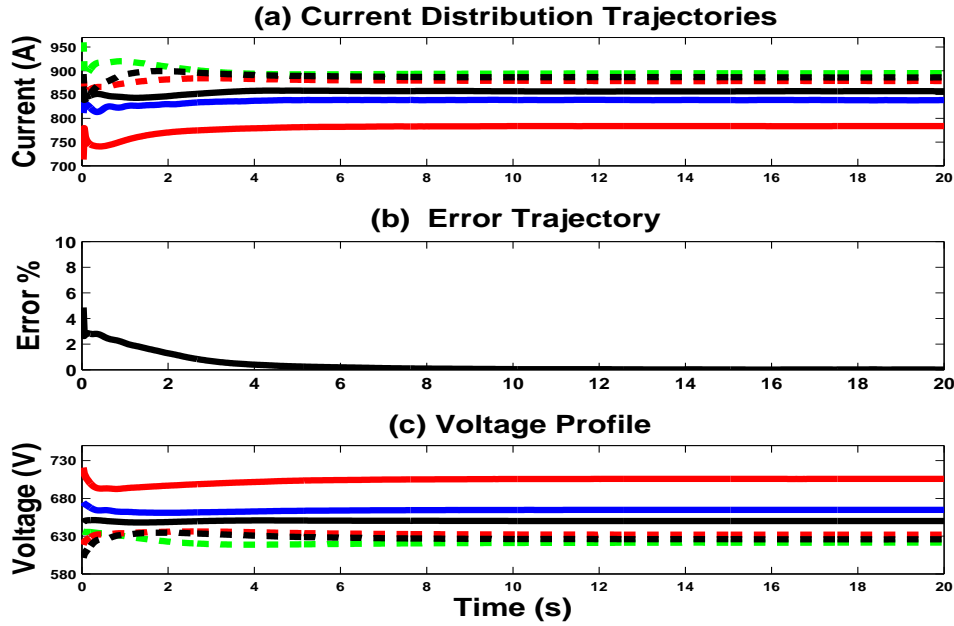Figure 24: Feeder currents, optimality error trajectory, and voltage profiles with tuned PI controllers

Table 3 shows the gain values for all controllers.

	Cntrlr. 1	Cntrlr. 2	Cntrlr. 3	Cntrlr. 4	Cntrlr. 5	Cntrlr. 6
K_P	0.00035	0.00008	0.00008	0.00008	0.0008	0.00008
K_I	0.0035	0.0008	0.0008	0.0008	0.008	0.0008

Table 3: PI controllers' gain values

4.5.4 Effect of Converters' Dynamics

Changing the dynamic of any of the converters will affect the system's behavior. The changes include the change in inductance, capacitance or any of the resistances. The effect ranges from introducing oscillation to the system's response to making the system unstable. Going back to the original case study, Fig.25 showcases the system's behavior when the inductance value of the second converter is changed to $L_2 = 1.81mH$.
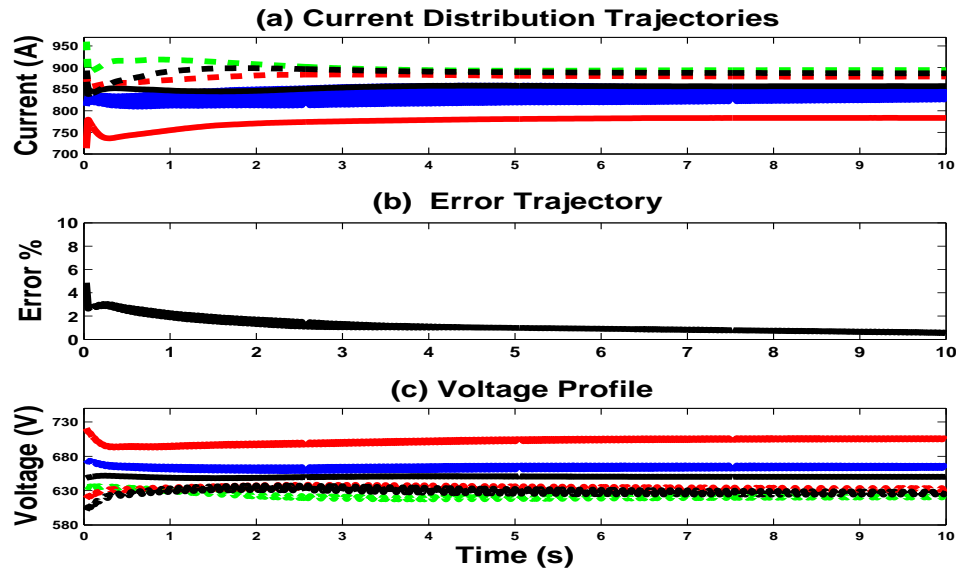

Figure 25: Feeder currents, optimality error trajectory, and voltage profiles when L_2 is changed

We can see that there is a large oscillation present in the feeder current of node 2 and the voltage profile of all the other nodes.

4.5.5 Step Size and Sampling Interval

In this part, the effect of sampling interval and step size on feeder currents and optimality error trajectories will be discussed. First, Fig. 26 shows the trajectories when the step size μ and the sampling interval τ are independent of each other (case 1). Noting that the step size type used is fixed step size.

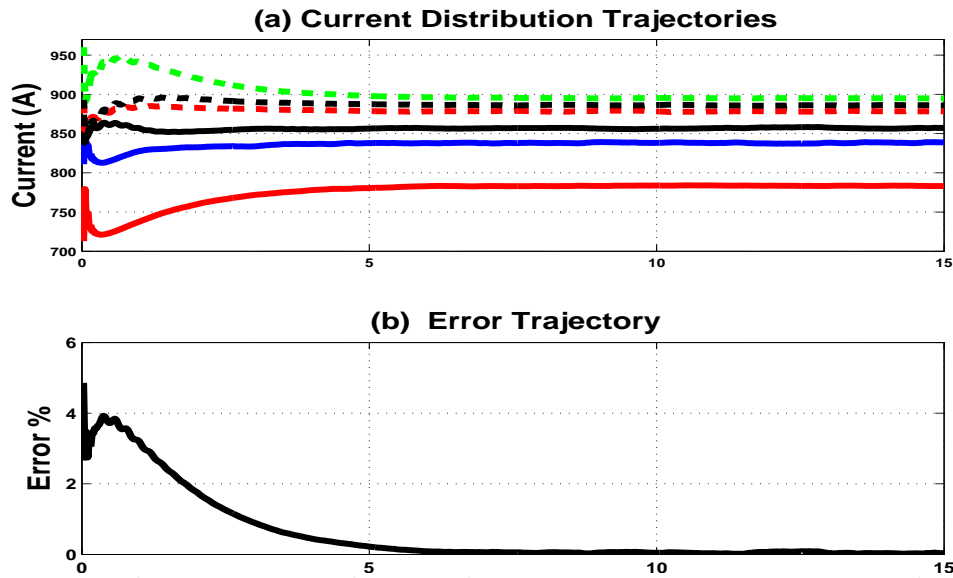Figure 26: Feeder currents, and optimality error trajectory, $\tau = 0.05$ and $\mu = 0.1$

When compared to the case in Fig.24 where τ is fixed and μ is dependent on τ (case 2) through the relation $(\alpha\mu = \tau)$, it is apparent from the error trajectories that the latter case converges faster to the optimal solution. Fig.27 shows the optimality error trajectories of both cases.
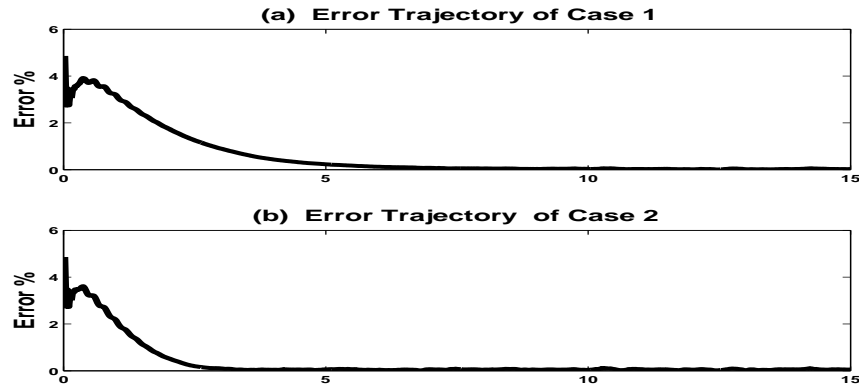
Figure 27: Optimality error trajectory for both cases of τ and μ selection.

It is clear that case 2 ,where there is a relation between τ and μ, has a faster convergence rate than the other case.

To further discuss the effect of sampling interval and step size on feeder currents and optimality error trajectories, different values of μ are tested by changing the value of α , and the selected values will be used to showcase the effect on the system's behavior. The value of τ is picked to be 0.05 for all cases.

Fig.28 shows the feeders' current trajectories and optimality error trajectory when $\alpha = 1$ and $\mu = \alpha\tau = 0.05$.
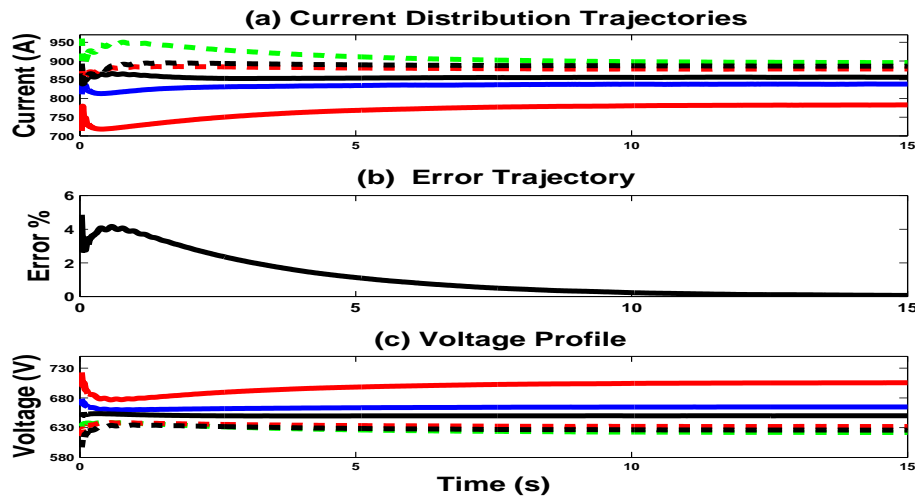
Figure 28: Feeders' current trajectories and optimality error trajectory for $\tau = 0.05$, $\alpha = 1$.

It is noticed from Fig.28 that the feeders' currents will converge to the optimal solution after a long period of time, which shows that the convergence rate for such case is slow.

In order to achieve faster convergence rate, a larger value for α will be selected $\alpha = 1/10$ and $\mu = 0.5$. Fig.29 shows the currents and error trajectories for this specific case.
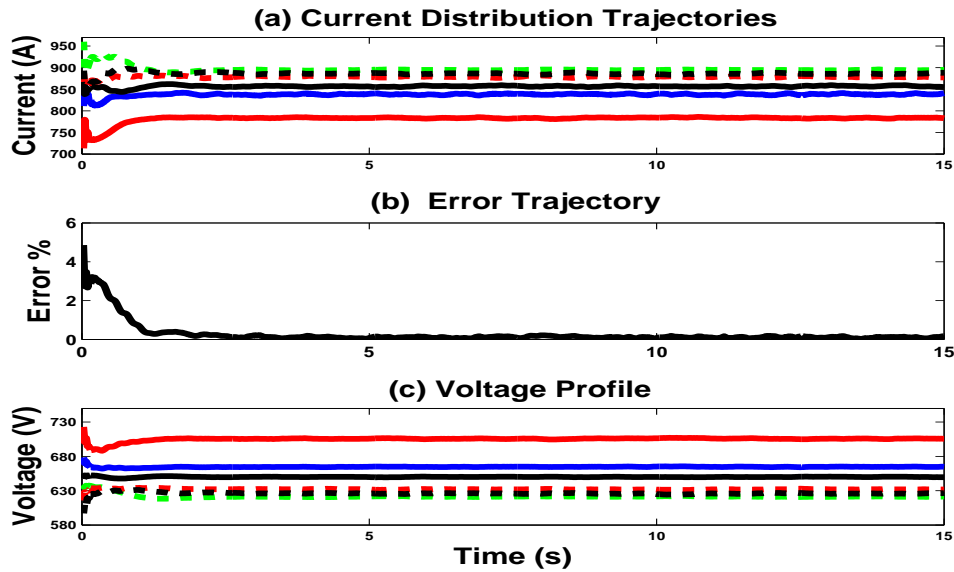
Figure 29: Feeders' current trajectories and optimality error trajectory for $\tau = 0.05$, $\alpha = 1/10$.

While the convergence rate in Fig.29 is faster compared to Fig.28, a small oscillation is started to merge on the system's response.

Next, an even larger value of $\alpha = 1/20$ will be picked to make the convergence rate faster. Fig.30 will the show the system's behavior for such a case noting that the step size $\mu = 1$.
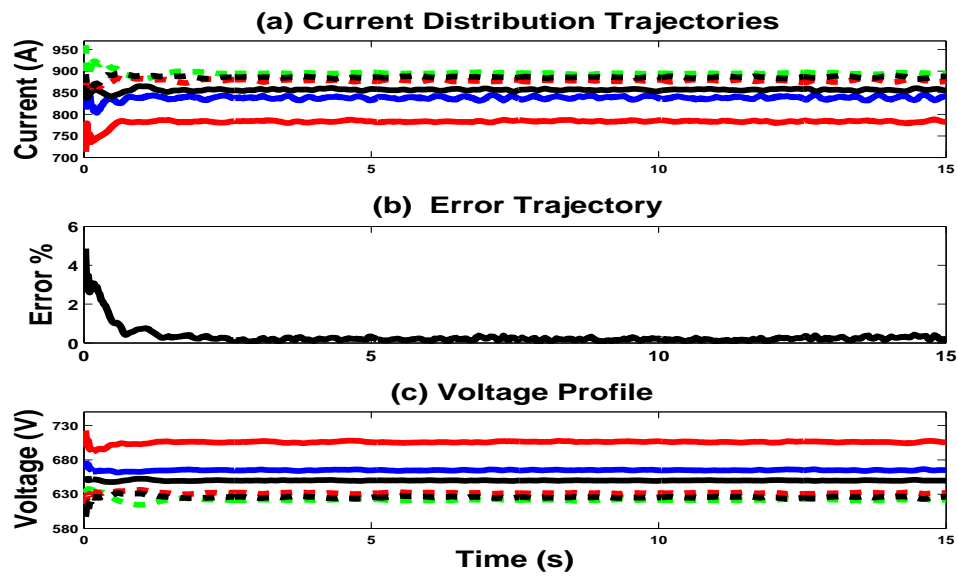
Figure 30: Feeders' current trajectories and optimality error trajectory for $\tau = 0.05$, $\alpha = 1/20$.

5 CONCLUSION AND FUTURE WORK

5 CONSCLUSION

The work in chapter 2 introduced a new control methodology for balancing feeder currents, reducing power loss, and maintaining acceptable voltage profiles. The methodology aims to achieve global optimization through distributed algorithms by using neighbor communications only. The recursive algorithms are shown to be convergent, asymptotically optimal, robust against load disturbances, and scalable with respect to node addition and deletion. The scalability is achieved without overwhelmingly increasing communication, control, or computational complexities.

By incorporating subsystem dynamics (physical systems) and integrating them with distributed optimization algorithms (in the cyberspace), the methodology in Chapter 3 presents a useful integration of cyber and physical systems. It is shown that coordination of cyber-physical systems is essential, in which the decision step size and the physical system's sampling rate must be selected together so that the resulting algorithms can be stable and convergent.

5 FUTURE WORK

There are several important open issues to be resolved in the future. The work done so far does not consider the costs of node power generation. Including such costs will be an interesting direction. Finally, it will be essential to study implementation issues such as costs on communication equipment, delays in operating power

electronics devices, data loss and latency in communication systems.

1. A distributed optimization strategy requires support from communication networks. Even though the utilization of such networks would improve the system's reliability, it always suffers from communication restraints. Those restraints could degrade the system's stability and performance. One of those restraints is the delay in operation of electronic devices. Therefore, the effects of communication delays on distributed control schemes for distributed optimal power and voltage management of DC microgrids comes to the motivation of this task. This distributed control strategy should accomplish a suitable tradeoff between the objectives.

2. Studying the effect of switching in DC microgrids and how we would reconfigure the optimization strategy accordingly. The motivation behind this topic is to develop the current control strategy so it can withstand the switching. For instance, if we would like to cut off a certain node from the grid for maintenance reasons, the developed distributed strategy would handle the switching without suffering from any stability or reliability issues.

3. In the problem formulation, the limits on line capacities are implicitly embedded in the term on the line costs which penalize large line currents. Similarly, the feeder line limits are implicitly embedded in supply current consensus (to be close to the average value) and the bus voltages (to be close to the rated voltage). For all these variables, it is possible to impose hard limits on them as inequality

constraints. As such, the optimization problems will be nonlinear and only numerical solutions can be pursued. The plan is to keep on investigating such practical constraints and nonlinear optimization and optimal control (including dynamics) in the future.

4. Finally, I would like to extend the current strategies to AC and hybrid AC/DC microgrids

REFERENCE

[1] Clark W. Gellings, Power to the people: New distribution technologies on the horizon, *IEEE Power and Energy Magazine*, vol. 9, no. 5, pp. 52-63, 2011.

[2] A. Keane and M. O'Malley, Optimal allocation of embedded generation on distribution networks, *IEEE Transactions on Power Systems*, vol. 20, no. 3, pp. 1640-1646, 2005.

[3] K. T. Tan, X. Y. Peng, P. L. So, Y. C. Chu, and M. Z. Q. Chen, Centralized Control for parallel operation of distributed generation inverters in microgrids, *IEEE Trans. Smart Grid*, vol.3, no.4, pp.1977-1987, Dec. 2012.

[4] M. M. A. Abdelaziz, M. F. Shaaban, H. E. Farag, and E. F. El-Saadany, A multistage centralized control scheme for islanded microgrids with PEVs, *IEEE Trans. Sustain. Energy*, vol. 5, no. 3, pp. 927-937, Jul. 2014.

[5] C. Ahn, and H. Peng, Decentralized and real-time power dispatch control for an islanded microgrid supported by distributed power sources, *Energies*, vol.6, pp. 6439-6454, 2013.

[6] K. Zhang, L. Xu, M. Ouyang, H. Wang, L. Lu, J. Li, and Z. Li, Optimal decentralized valley-filling charging strategy for electric vehicles, *Energy Convers. Manage.*, vol.78, pp.537-550, Feb. 2014.

[7] M. Babazadeh and H. Karimi, Robust decentralized control for islanded operation of a microgrid, in *Proc. IEEE Conf. Power Energy Soc. Gener. Meet.*, San Diego, CA, USA, 2011, pp.1-8.

[8] H. Dagdougui and R. Sacile, Decentralized control of the power flows in a network of smart microgrids modeled as a team of cooperative agents, *IEEE Trans. Control Syst. Technol.*, vol.22, no.2, pp.510-519, Mar. 2014.

[9] H. Lan, S. Wen, Q. Fu, D. C. Yu, and L. Zhang, Modeling analysis and improvement of power loss in microgrid, *Math. Probl. Eng.*, vol. 2015, 2015, Art ID. 493560.

[10] Z. Mahmoodzadeh, N. Ghanbari, A. Mehrizi-Sani, and M. Ehsan, Energy loss estimation in distribution networks using stochastic simulation, in *Proc. IEEE Conf. Power Energy Soc. Gener. Meet.*, Denver, CO, USA, 2015, pp. 1-5.

[11] S. Gopiya Naik, D.K. Khatod, and M.P. Sharma, Optimal allocation of combined DG and capacitor for real power loss minimization in distribution networks, *Electr. Power Energy Syst.*, vol. 53, pp. 967-973, Dec. 2013.

[12] L. K. Vedulla and M. K. Mishra, "PSO based power sharing scheme for an islanded DC microgrid system,*IECON 2017 - 43rd Annual Conference of the IEEE Industrial Electronics Society*, Beijing, 2017, pp. 392-397. doi: 10.1109/IECON.2017.8216070

[13] K. Clement-Nyns, E. Haesen, and J. Driesen, The impact of charging plug-in hybrid electric vehicles on a residential distribution grid, IEEE Trans. Power Syst., vol. 25, no. 1, pp. 371-380, Feb. 2010.

[14] P. Alluri, J. Solanki, S. K. Solanki, Charging coordination of plug-in electric vehicles based on the line flow limits and power losses, in *Proc. IEEE Intl. Conf. Technol. Adv. Power Energy*, Kollam, India, 2015, pp. 233-238.

[15] C. Wei, Sendai, Z. Md Fadlullah, N. Kato, and I. Stojmenovic, A novel distributed algorithm for power loss minimizing in smart grid, in *Proc. IEEE Conf. Smart Grid Comm.*, Venice, Italy, 2014, pp. 290-295.

[16] A.P. Lopes, C.L. Moreira, and A.G. Madureira, Defining control strategies for MicroGrids islanded operation, *IEEE Transactions on Power Systems*, vol. 21, no. 2, pp. 916-24, 2006.

[17] Robert H. Lasseter, Smart distribution: Coupled microgrids, Smart grid: The electric energy system of the future, *Proceedings of the IEEE*, vol. 99, no. 6, pp. 1074-1082, 2011.

[18] Q. Xu, J. Xiao, P. Wang and C. Wen, "A Decentralized Control Strategy for Economic Operation of Autonomous AC, DC, and Hybrid AC/DC Microgrids," *IEEE Transactions on Energy Conversion*, vol. 32, no. 4, pp. 1345-1355, Dec. 2017. doi: 10.1109/TEC.2017.2696979

[19] Huanhai Xin, Zhihua Qu, J. Seuss, and A. Maknouninejad, A self-organizing strategy for power flow control of photovoltaic generators in a distribution network, *IEEE Transactions on Power Systems*, vol. 26, no. 3, pp. 1462-73, 2011.

[20] A. Engler, N. Soultanis, Droop control in LV-grids, *2005 International Conference on Future Power Systems*, pp. 6-18, 2005.

[21] R. Tonkoski, L.A.C. Lopes, T.H.M. El-Fouly, Coordinated active power curtailment of grid connected PV inverters for overvoltage prevention, *IEEE Transaction on Sustainable Energy*, vol. 2, no.2, pp. 139-147, 2011.

[22] A. Korompili and A. Monti, "Analysis of the dynamics of dc voltage droop controller of dc-dc converters in multi-terminal dc grids," *2017 IEEE Second International Conference on DC Microgrids (ICDCM)*, Nuremburg, 2017, pp. 507-514. doi: 10.1109/ICDCM.2017.8001094

[23] R. P. Nair and P. Kanakasabapathy, "Control of a DC microgrid under dynamic load condition," *2017 International Conference on Technological Advancements in Power and Energy (TAP Energy)*, Kollam, 2017, pp. 1-6. doi: 10.1109/TAPENERGY.2017.8397212

[24] D. Pudjianto, C.Ramsay, and Goran Strbac, Microgrids and virtual power plants: Concepts to support the integration of distributed energy resources, *Proceedings of the Institution of Mechanical Engineers*, Part A: Journal of Power and Energy, vol. 222, no. 7, pp. 731-741, 2008.

[25] P. Tenti, H.K.M. Paredes, and P. Mattavelli, Conservative Power Theory, a Framework to Approach Control and Accountability Issues in Smart Microgrids, *IEEE Transactions on Power Electronics*, vol. 26, no. 3, pp. 664-73, 2011.

[26] Aris L. Dimeas and Nikos D. Hatziargyriou, Operation of a Multiagent System for Microgrid Control, *IEEE Transactions on Power Systems*, vol. 20, no. 3, pp. 1447-1455, 2005.

[27] G. Rigatos, P. Siano, and N. Zervos, A Distributed State Estimation Approach to Condition Monitoring of Nonlinear Electric Power Systems, *Asian Journal of Control*, vol 15, no. 3, pp. 849860, 2013.

[28] J. Hu, J. Duan, H. Ma and M. Chow, Distributed Adaptive Droop Control for Optimal Power Dispatch in DC Microgrid, *IEEE Transactions on Industrial Electronics*, vol. 65, no. 1, pp. 778-789, Jan. 2018. doi: 10.1109/TIE.2017.2698425

[29] L. Meng, T. Dragicevic, J. M. Guerrero and J. C. Vasquez, Dynamic consensus algorithm based distributed global efficiency optimization of a droop controlled DC microgrid, *2014 IEEE International Energy Conference (ENERGYCON)*, Cavtat, 2014, pp. 1276-1283. doi: 10.1109/ENERGYCON.2014.6850587

[30] Tielong Shen, Romeo Ortega, Qiang Lu, Shengwei Mei and Katsutoshi Tamura, Adaptive L_2 disturbance attenuation Of Hamiltonian systems with parametric perturbation and application to power systems, *Asian Journal of Control*, vol. 5, no. 1, pp. 143152, 2003.

[31] L. Y. Wang, C. Wang, G. Yin, and Y. Wang, Weighted and constrained consensus for distributed power dispatch of scalable microgrids, *Asian J. Control*, vol. 17, no. 5, pp. 1725-1741, Sep. 2015.

[32] M. B. Shadmand and R. S. Balog, "Multi-Objective Optimization and Design of Photovoltaic-Wind Hybrid System for Community Smart DC Microgrid,*IEEE Transactions on Smart Grid*, vol. 5, no. 5, pp. 2635-2643, Sept. 2014. doi: 10.1109/TSG.2014.2315043

[33] L. Yu, T. Jiang, and Y. Cao, Energy cost minimization for distributed internet data centers in smart microgrids considering power outages, *IEEE Trans. Par. Distr. Syst.*, vol. 26, no. 1, pp. 120-130, Jan. 2015.

[34] M. Esmailia, E. C. Firozjaee, and H. A. Shayanfar, Optimal placement of distributed generations considering voltage stability and power losses with observing voltage-related constraints, *Appl. Energy*, vol. 113, pp. 1252-1260, Jan. 2014.

[35] M. M. Aman, G. B. Jasmon, A. H. A. Bakar, and H. Mokhlis, A new approach for optimum DG placement and sizing based on voltage stability maximization and minimization of power losses, *Energy Convers. Manage.*, vol. 70, pp. 202-210, Jun. 2013.

[36] P. Kayal and C. K. Chand, Placement of wind and solar based DGs in distribution system for power loss minimization and voltage stability improvement, *Electr. Power Energy Syst.*, vol. 53, pp.795-809, Dec. 2013.

[37] R. Srinivasa Rao, K. Ravindra, K. Satish, and S. V. L. Narasimham, Power loss minimization in distribution system using network reconfiguration in the presence of distributed generation, *IEEE Trans. Power Syst.*, vol. 28, no. 1, pp. 317-325, Feb. 2013.

[38] S. Biswas, S. K. Goswami, and A. Chatterjee, Optimum distributed generation placement with voltage sag effect minimization, *Energy Convers. Manage.*, vol. 53, pp. 153-174, Jan. 2012.

[39] D. Zhang, J. Jiang, L. Y. Wang, and W. Zhang, Robust and scalable management of power networks in dual-source trolleybus systems: A consensus control framework, *IEEE Trans. Intel. Trans. Syst.*, vol. 17, no. 4, pp. 1029-1038, April 2016.

[40] D. Zhang, L. Wang, J. Jiang, and W. Zhang, Optimal Power Management in Dual-Source Trolleybus Systems, *IEEE Trans. Intel. Trans. Syst.*, vol. 19, no. 4, pp. 1188-1197, April 2018.

[41] "Microgrids — Grid Modernization — NREL", *Nrel.gov*, 2017. [Online]. Available: https://www.nrel.gov/grid/microgrids.html. [Accessed: 14- Oct- 2017].

[42] Campbell, Richard J. Weather Related Power Outages and Electric System Resiliency. Report for Congress, Washington, D.C. Congressional Research Service, 2012.

[43] N. Lidula and A. Rajapakse, "Microgrids research: A review of experimental microgrids and test systems", *Renewable and Sustainable Energy Reviews*, vol. 15, no. 1, pp. 186-202, 2011.

[44] M Quashie, G Joos, "A methodology to optimize benefits of microgrids," Power and Energy Society General Meeting (PES), 2013.

[45] D. Vine, D. Attanasio and E. Shittu, "MICROGRID MOMENTUM: BUILD-ING EFFICIENT, RESILIENT POWER", *The Center for Climate and Energy Solutions Technology*, pp. 1-3, 2017.

[46] J. Rey, P. Vergara, G. Osma, and G. Ordez, "Considerations for the Design and Implementation of Microgrids", *VII Simposio Internacional sobre la Calidad de la Energa Elctrica*, Medellin, Colombia, 2013.

[47] O. Veneri, *Technologies and Applications for Smart Charging of Electric and Plug-in Hybrid Vehicles*. Cham: Springer International Publishing, 2017, p. 41.

[48] "Solar Industry Data — SEIA", *SEIA*, 2017. [Online]. Available: https://www.seia.org/solar-industry-data. [Accessed: 15- Oct- 2017].

[49] "Kamuthi Solar PV Power Plant India - GEO", *Globalenergyobservatory.org*, 2017. [Online]. Available: http://globalenergyobservatory.org/geoid/46233. [Accessed: 15- Oct- 2017].

[50] M. Ton, B. Fortenbery, and W. Tschudi. DC power for improved data center efficiency. 2008.

[51] J. Miller, "Power System Optimization Smart Grid, Demand Dispatch and Microgrids", National Energy Technology Laboratory, 2011.

[52] T. Weise, *Global Optimization Algorithms Theory and Application-*, 2nd ed. 2009.

[53] M. Lin, J. Tsai and C. Yu, "A Review of Deterministic Optimization Methods in Engineering and Management",*Mathematical Problems in Engineering*, vol. 2012, pp. 1-15, 2012. Available: 10.1155/2012/756023.

[54] J.C Spall, *Introduction to Stochastic Search and Optimization: : Estimation, Simulation, and Control*. Wiley, 2003, pp. 19-27.

[55] D. Molzahn, F. Dorfler, H. Sandberg, S. Low, S. Chakrabarti, R. Baldick and J. Lavaei, "A Survey of Distributed Optimization and Control Algorithms for Electric Power Systems", *IEEE Transactions on Smart Grid*, vol. 8, no. 6, pp. 2941-2962, 2017.

[56] G. Coulouris, J. Dollimore, T. Kindberg and G. Blair, *Distributed systems Concepts and Design*, 5th ed. Boston: Addison-Wesley, 2012.

[57] S. Ghosh, *Distributed systems An Algorithmic Approach*, 2nd ed. Boca Raton: Chapman & Hall/CRC, 2007

[58] G. Yin, L. Y. Wang, Y. Sun, D. Casbeer, R. Holsapple, and D. Kingston, Asymptotic optimality for consensus-type stochastic approximation algorithms using iterate averaging, *J. Control Theory Appl.*, vol.11, no.1, pp.1-9, Feb. 2013.

[59] H. J. Kushner, and G. Yin, Stochastic Approximation and Recursive Algorithms and Applications, 2nd ed. New York, NY, USA: Springer-Verlag, 2003.

ABSTRACT

DISTRIBUTED OPTIMAL POWER AND VOLTAGE MANAGEMENT IN DC MICROGRIDS

by

EYAD A SINDI

December 2019

Advisor: Dr. Le Yi Wang

Major: Electrical Engineering

Degree: Doctor of Philosophy

The work developed new control strategies to address fundamental issues of power balance, line loss reduction, and voltage profile management in DC microgrids. In microgrids of distributed renewable generations and controllable loads, load allocation to different distributed generators, line losses, voltage stability and quality are intimately coupled, departing significantly from traditional power grids in which economic dispatch and voltage stability are typically separate control tasks.

In this work, a multi-objective optimization strategy is introduced to address the challenges imposed by these coupled issues. Global optimal solutions are derived. Recursive optimization algorithms for distributed control strategies are introduced and shown to converge to the global optima. Case studies using DC-powered trolley-bus systems are conducted to evaluate the algorithms, showcasing their convergence, ability to function under scalable networks, and robustness to load perturbations.

Finally, the work develops optimal control strategies for management of DC microgrids including subsystem dynamics. The inclusion of subsystem dynamics accounts for many real systems, especially converter dynamics, impacts performance significantly, and complicates system analysis. A comparison to the trolley bus system without the inclusion of subsystem dynamics was part of the case studies. Additionally, case studies covering the effect of controllers and dynamics of the DC-DC converter are conducted to evaluate the modified algorithm. Sampling interval and step size effects on the system's behavior were also discussed.

AUTOBIOGRAPHY

Education:

- Current Ph.D. student at Wayne State University, Electrical Engineering Department, since August 29th, 2015.

- Master of Science in Electrical Engineering from Wayne State University, Detroit, Michigan, United States, Fall 2015.

- Bachelor of Science in Electrical Engineering from King Abdulaziz University, Jeddah, Saudi Arabia, Fall 2008.

Work Experience:

- Electromechanical Inspector, Maintenance & UtilityDepartment, King Abdulaziz International Airport (KAIA), from 03-2009 to 12-2011

- Electrical Engineer, Engineering Services Deaprtment, SAFARICO. from 14-10-2008 to 29-2-2009.

Publications:

- E. Sindi, L. Wang, M. Polis, G. Yin and L. Ding, "Distributed Optimization in DC Microgrids with Subsystem Dynamics", *The 2019 8th International Conference on Systems and Control (ICSC'2019)*, Marrakesh, Morocco, 2019. Accepted.

- E. Sindi, L.Y. Wang, M. Polis, G. Yin, and L. Ding, " Distributed Optimal Power and Voltage Management in DC Microgrids: Applications to Dual-Source Trolleybus Systems", *IEEE Transactions on Transportation Electrification*, 4(3), pp.778-788, June 2018.

- E. Sindi, L. Wang, M. Polis, G. Yin and L. Ding, "Distributed Optimal Power and Voltage Management in DC Microgrids", in *2017 SIAM Conference on Control and Its Applications*, Pittsburgh, 2017.

- L. Ding, Q. Han, L. Y. Wang and E. Sindi, "Distributed Cooperative Optimal Control of DC Microgrids With Communication Delays," *IEEE Transactions on Industrial Informatics*, vol. 14, no. 9, pp. 3924-3935, Sept. 2018. doi: 10.1109/TII.2018.2799239